

STUDY OF DOPAMINE-DIAZEPAM BIOMOLECULAR COMPLEX USING IEFPCM MODEL AND SPECTROSCOPIC TECHNIQUES

Lamthaka Willingson¹ and Th. Gomti Devi^{*1}

¹Department of Physics, Manipur University, Canchipur 795003, Manipur, India *Corresponding Author: tgd@manipuruniv.ac.in

(Received 3 December 2024; revised 15 January 2025; accepted 31 January 2025; published 7 April 2025)

Abstract: Diazepam is a benzodiazepine class of drugs significantly used for treating neurotic disorders such as anxiety, acute recurrent seizures, alcohol detoxification, spasticity, and severe muscle spasms. Several researchers have shown that diazepam greatly influences the level of dopamine in the human body, as It is a crucial neurotransmitter that plays a vital role in avoiding neurological disorders. The present research work focuses on understanding the vibrational and spectroscopic study of the Dopamine – Diazepam biomolecular complex. The theoretical analysis is performed using Density Functional Theory (DFT), B3LYP/6-311++G(d,p) level of theory with the integral equation formalism polarizable continuum model (IEFPCM). The optimized structure of the biomolecular complex is determined using Gaussview 6.0 and Gaussian16. Vibrational Energy Distribution Analysis (VEDA) was employed for vibrational analysis. Molecular docking simulations of the biomolecular complex of the docked protein-ligand system were performed to gain deeper insights into the mechanism. A good agreement was observed between the computational and experimental vibrational frequencies.

Keywords: Density Functional Theory; HOMO-LUMO; Raman spectroscopy; XRD spectroscopy; Molecular Docking simulation

PACS: PACS: 33.15.-e, 87.15.K-, 82.80.-d, 33.15.Mt

1 Introduction

Neurotic disorders are primarily linked to stress, maladaptive stress responses, and individual susceptibility to anxiety [1]. Notably, stress and coping are closely tied to socio-cultural factors, which influence symptom presentation, illness perception, and help-seeking behavior [2, 3]. Cultural background also shapes how physicians interpret symptoms and assign meaning to illnesses, affecting the epidemiology, phenomenology, and treatment outcomes of psychiatric disorders, particularly anxiety disorders. Anxiety is a normal human emotion that, in moderation, promotes anticipatory and adaptive responses to challenging or stressful situations [4]. It encompasses behavioral, emotional, and cognitive responses to perceived danger. Anxiety is a normal human emotion that, in moderation, promotes anticipatory and adaptive responses to challenging or stressful situations. However, when excessive, it can destabilize an individual, leading to a dysfunctional state. Anxiety is deemed excessive or pathological when it occurs without a clear challenge or stressor, is disproportionate in duration or intensity, causes significant distress, or results in impairments in psychological, social, occupational, or biological functioning [5]. Anxiety is an unpleasant physiological state characterized by an exaggerated response to certain situations. Research suggests that multiple brain regions, including the amygdala, hippocampus, and frontal cortex, are involved in the modulation and expression of anxiety. Dysregulation of neurotransmitters and their receptors has been linked to mood disorders such as anxiety. Notably, Dopamine plays a significant role in anxiety regulation across different brain areas. Evidence indicates that the mesolimbic, mesocortical, and nigrostriatal Dopaminergic systems are implicated in anxiety, with both Dopamine D1 and D2 receptors contributing to its modulation



[6]. The activity of the Dopaminergic system is influenced by various neurotransmitters, including glutamatergic neurons from the medial prefrontal cortex (mPFC), GABAergic fibers from the nucleus accumbens (NAc) and ventral pallidum, as well as cholinergic inputs from the pedunculopontine and laterodorsal tegmental nuclei. Consequently, alterations in glutamatergic and GABAergic signaling, along with changes in the Dopaminergic transmission within the mesolimbic, mesocortical, and nigrostriatal pathways, may contribute to anxiety-like behaviors.

Dopamine, an essential catecholamine neurotransmitter, is widely distributed across various biological systems. It is synthesized in the brain's ventral tegmental area, substantia nigra, and hypothalamus, where it performs numerous critical physiological functions in humans. Dopamine imbalances, whether as a deficiency or an excess, are associated with various neurological disorders, including Parkinson's disease, schizophrenia, autism, anxiety, and attention deficit hyperactivity disorder (ADHD) [7]. Interestingly, increased Dopamine levels have been linked to mild anxiety and depression in young adults [8]. Furthermore, Dopamine plays a crucial role in learning, motor control, motivation, and attention. As a result, significant efforts are focused on developing simple and sensitive methods for directly quantifying Dopamine levels. However, detecting Dopamine within the brain and body remains a challenging task leading to difficulty in early disease detection and monitoring, and the disorders often go unrecognized and untreated. Research by Borwin Bandelow et al. [9] highlights that anxiety disorders, including panic disorder (with or without agoraphobia), generalized anxiety disorder, social anxiety disorder, specific phobias, and separation anxiety disorder, are among the most common mental health conditions. These disorders significantly impact public health, imposing a high disease burden and substantial healthcare costs. Large-scale surveys estimate that up to 33.7% of individuals experience an anxiety disorder during their lifetime. Typically chronic, their prevalence tends to decline with age, but they often co-occur with each other and other mental health conditions. Historically, early anxiety treatments relied on general depressants and sedatives such as alcohol, opiates, lithium bromide, and chloral hydrate [10]. By the mid-20th century, these were replaced by carbamates and barbiturates. A major milestone in anxiety pharmacotherapy was the introduction of benzodiazepines, starting with chlordiazepoxide (Librium) in 1960. This drug offered improved safety and a wider therapeutic range compared to its predecessors. The launch of Diazepam in 1963 further advanced treatment, providing strong anxiolytic effects with fewer sedative properties. Diazepam, initially used for anxiety, was also effective for epilepsy, muscle spasms, and alcohol withdrawal. Despite a limited understanding of its mechanism for years, its efficacy made it widely popular [11, 12]. Notably, unlike most drugs of abuse that increase Dopamine release in the nucleus accumbens, Diazepam has been shown to decrease Dopamine release [13]. Benzodiazepines, including Diazepam, function as positive allosteric modulators of the GABA receptor complex, binding to a specific site at the alpha-gamma subunit interface. This binding enhances chloride-ion influx upon GABA activation, hyperpolarizing postsynaptic membranes and amplifying the central nervous system's response to endogenous GABA [14, 15]. These effects, particularly in the limbic system, thalamus, hypothalamus, and cerebral cortex, underlie the calming effects of benzodiazepines [16]. Diazepam's actions in these brain regions contribute to its anxiolytic and antiepileptic properties. Its potency, excellent bioavailability, and rapid onset of action make it clinically effective and commercially viable. However, these same qualities also increase the risk of dependence and misuse, prompting regulatory measures to limit benzodiazepine prescriptions. Long-term use has been associated with a heightened risk of dependence and withdrawal, leading to a shift in therapeutic approaches toward monitoring and mitigating these risks [16].

Studies indicate that Dopamine exhibits diverse molecular properties, particularly in its hydrochloride salt form, where protonation enhances stability [17]. Dopamine hydrochloride forms hydrogen bonds with solvents like water, ethanol, and urea, interacting through $C-H\cdots\pi$, $\pi\cdots\pi$ stacking, and hydrogen bonding with nicotinamide, boosting electron density around its benzene ring and enhancing p- π conjugation with phenolic hydroxyl groups [18, 19]. Additionally, Dopamine can synergize with other drugs; for example, its coadministration with dextrorphan enhances antinociceptive effects [20]. Studies also highlight hydrogen bonding and hydrophobic interactions in Dopamine complexes with bovine serum albumin, β -cyclodextrin, and glycine [21, 22, 23]. Moreover, the literature survey suggests that Diazepam can form a complex through hydrogen bonding with charge transfer to enhance its broad spectrum of effects, including antianxiety, sedative and sleep-inducing, anticonvulsive, and muscle relaxation properties. Diazepam is effectively absorbed from the gastrointestinal tract in its unchanged form and is then metabolized in the liver after oral administration [24, 25, 26, 27, 28, 29, 30, 31, 32].

Despite extensive research, quantum chemical and spectroscopic studies of the Dopamine-Diazepam complex using Density Functional Theory (DFT) combined with the Integral Equation Formalism Polarizable Continuum Model (IEFPCM) remain unexplored. Given Dopamine's stimulant effects and Diazepam's calming properties, this study investigates their molecular interactions and spectral behavior using DFT calculations and techniques such as FTIR, Raman, and powder X-ray diffraction. Anxiety disorders and neurotic disorders often involve



overlapping symptoms like dysregulated mood, motor tension, and cognitive issues. A hybrid drug might simultaneously alleviate these symptoms more comprehensively. A hybrid approach might allow for lower doses of both components, potentially reducing side effects associated with higher doses of Diazepam (e.g., sedation, dependency). Patients unresponsive to traditional anxiolytics or antidepressants might benefit from this new mechanism of action. Our methodology includes molecular docking using Autodock, visualized with Discovery Studio, and quantum mechanical calculations such as Frontier Molecular Orbital (FMO), Natural Bond Orbital (NBO), Nonlinear Optical (NLO), Atoms in Molecules (AIM), and Non-Covalent Interaction (NCI) analysis. Toxicity and drug-likeness assessments further validate the biomolecular complex. By integrating computational modeling and spectroscopy, this study provides insights into the potential of Dopamine-Diazepam interactions, paving the way for innovative treatments for neurological disorders and substance abuse.

2 Materials and Methods

2.1 Experimental methods

The Dopamine hydrochloride (purity: $\geq 98\%$) is obtained from Sisco Research Laboratories Private Limited, and the Diazepam and distilled water are from the local pharmacy. Dopamine hydrochloride and Diazepam are ground thoroughly and mixed in the 1:1:2 molar ratio in distilled water to form a biomolecular complex. A 1:1 stoichiometry indicates a specific interaction between Dopamine and Diazepam, where one molecule interacts directly with one Diazepam. This ratio is typical in scenarios where molecular complementarity—shape, charge, and thermodynamic properties—ensures a tight and selective interaction [33, 34]. The 1:1 ratio is significant in the human biological systems because it allows for balanced modulation of pathways. For instance, Excessive Dopamine could lead to excitatory effects, such as anxiety or agitation. Diazepam counteracts such effects by potentiating inhibitory GABA signaling. A 1:1 interaction could represent an optimized balance that reduces the risk of dysregulation in neurotransmitter systems. The biomolecular complex is warmed up for a while using a heating mantle to vapourize the water [35]. The Spectrum Two FT-IR Spectrometer, PerkinElmer, 0.5 cm⁻¹ resolution and range from 400-4000 cm⁻¹ is used to record FTIR spectra [36, 37]. Moreover, the Raman spectra of the biomolecular complex are taken within the range of 200-4000 cm⁻¹ with the help of MRIe Table Top Micro Raman Spectrometer, Protrustech Corporation Limited, Taiwan, which has a laser of 785 nm excitation source and a standard spectral resolution of 1.8 cm⁻¹. The possible cocrystal formation of the biomolecular complex is examined with the help of an X'pert pro-X-ray diffractometer, which has radiation wavelength, $\lambda=$ 1.541874 Å in the $10^{\circ}-90^{\circ}(2\theta)$ range employing a step size of 0.03 Å. The phase identification of the interacting complex is performed using Match! 3 software [38]. Using Origin Pro 2021 software, both experimental and theoretical spectra are analysed.

2.2 Computational details

The initial step involves optimizing the structure of Dopamine-Diazepam in the gas phase using Gaussian 16 software, employing the DFT/B3LYP/6-311++G(d,p) level of theory with IEFPCM model, and computational work is facilitated by Gaussview 6.0 [39, 40]. The scaling factor of 0.9668 is multiplied at the calculated vibrational frequencies to compensate for systematic errors like anharmonic vibrational frequencies, basis set incompleteness, and electron correlation [41, 42]. The choice of the DFT/B3LYP/6-311++G(d,p) level of theory is motivated by its provision of a split-valence triple-zeta basis set, encompassing functions for describing both core and valence orbitals, along with polarization functions (d,p) to accurately depict chemical bonds, particularly in heavy atoms and hydrogen. Including diffuse functions, denoted by "+", aids in describing anions and longrange interactions like dispersion and hydrogen bonds. Furthermore, the hybrid B3LYP/6–311++G(d,p) function is commonly favored for investigating hydrogen bonding interactions in self-assembling and biochemical materials, proving to be one of the most effective basis sets for obtaining optimal results [43]. The research work utilized the implicit solvation model: the integral equation formalism polarizable continuum model (IEFPCM) with water as the solvent. These models simulate the solvent's effect by embedding the molecule of interest within a cavity, where the surface charge is stabilized according to the dielectric constant of the chosen solvent [44, 45, 46]. IEFPCM treats the solvent as a uniform dielectric medium (ϵ) surrounding the solute in a cavity where IEFPCM represents the solute with a cavity formed by interconnected spheres, each sphere's radius corresponding to the atomic radii of the solute in which the uniform dielectric medium interacts with the wavefunction of the solute [47, 48]. Comparative analysis reveals that B3LYP DFT calculations yield a lower RMSD value, indicating



its reliability concerning self-consistent field (SCF) energy and RMSD value [49]. VEDA software determines vibrational assignments and potential energy distribution (PED), while Raman activity is converted into Raman intensity via Gaussum 3.0 software [50, 51, 52, 53, 54, 55]. Online SwissADME evaluates the drug-likeness of the Dopamine-Diazepam biomolecular complex [56]. Molecular docking is conducted using the Autodock [57]. Biovia discovery software [58] offers insights into protein-ligand interactions with minimum binding energy. Noncovalent interaction (NCI) analysis, Atoms in molecules (AIM) exploring interactions such as steric effects, hydrogen bonds, van der Waals forces, and hydrophobic interactions, is performed using Multiwfn and VMD software [59, 60]. Finally, Protox II software is employed for toxicity determination [61].

3 Results and Discussion

3.1 Analysis of structural parameters

The optimized structure of the Dopamine – Diazepam biomolecular complex is displayed in figure 1. The geometrical characteristics, viz., bond lengths, and bond angles, which are computed, are summarized in table 1. The optimized structure of the Dopamine – Diazepam biomolecular complex, displayed a total of 57 (fifty-seven) bond lengths with twenty-three C-C bonds with bond lengths ranging from 1.383-1.534Å, twenty C-H bonds with a bond length range of 1.082–1.098Å, two N-H bonds with bond lengths of 1.016 Å each, six C-N bonds with bond length ranging from 1.284–1.472 Å, three C-O bonds with bond length ranging from 1.225–1.376 Å, two O-H bonds with a bond length of 0.965 Å and 0.968 Å, and one C-Cl bond serving as the longest bond length in the biomolecular complex with 1.764Å. The monomeric units form intermolecular hydrogen bonding at $(H^{11} - C^{l40})$ and $(O^{12} - H^{54})$ with bond lengths of 2.855Å and 2.533Å. The biomolecular complex exhibits three double bonds at $(C^{31} = C^{30})$, $(C^{25} = O^{39})$, and $(C^{24} = N^{33})$ having bond lengths of 1.383Å, 1.225Å, and 1.284Å. The biomolecular displays eighty-six bond angles ranging from 106.106°-124.100°. The bond lengths of (H²⁰-N¹⁹) and (C¹⁶-N¹⁹) in the dopamine monomer are 1.016 Å and 1.468 Å, respectively, and decrease slightly to 1.015 Å and 1.472 Å upon forming a biomolecular complex (Table S-1 in appendix A and Table 1). Notably, the $(O^{10}-H^{11})$ and $(O^{12}-H^{13})$ bonds in dopamine, which play a critical role in intermolecular hydrogen bond formation within the complex, also exhibit slight length increases from 0.966 Å and 0.962 Å to 0.968 Å and 0.965 Å, respectively (table S-1 in appendix A and table 1). Conversely, significant changes are observed in the computed bond lengths of (C^8-Cl^{18}) in diazepam, a key contributor to intermolecular hydrogen bonding in the complex, which increases from 1.757 Å to 1.764 Å, while the (C^7-H^{32}) bond length remains unchanged (table S-1 in appendix A and table 1). Additionally, the carboxyl group $(C^3 = O^{17})$ in the diazepam monomer shows an increase in bond length from 1.214 Å to 1.225 Å within the complex (table S-1 in appendix A and table 1). However, the (C^1-H^{31}) bond length of the diazepam molecule decreases slightly, from 1.100 Å to 1.098 Å, in the biomolecular complex. These variations in bond lengths within the optimized monomers upon molecular complex formation indicate potential charge transfer (table S-2 in appendix A) and shifts in vibrational frequencies (table 7), driven by the establishment of intermolecular hydrogen bonds within the complex.

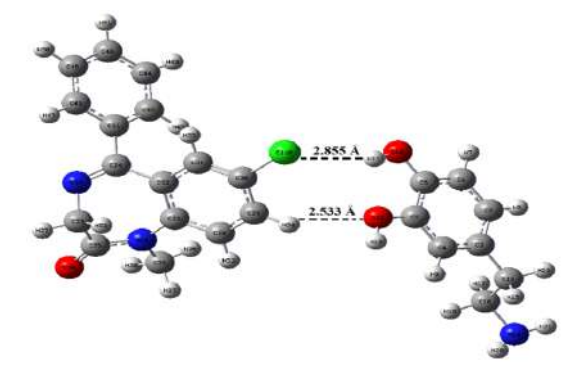


Figure 1: Optimized structure of Dopamine – Diazepam biomolecular complex



| 10 10 10 10 10 10 10 10 |
|---|
| N ¹⁹ - H ²⁰ 110.032 C ¹⁶ - H ¹⁸ 107.912 C ¹⁶ - H ¹⁷ 113.000 C ¹⁶ - H ¹⁷ 106.957 C ¹⁶ - C ¹⁴ 108.888 |
| $\begin{array}{cccc} C^{16} - H^{18} & 107.912 \\ & & & & & \\ C^{16} - H^{17} & 113.000 \\ & & & & \\ C^{16} - H^{17} & 106.957 \\ & & & & \\ C^{16} - C^{14} & 108.888 \\ & & & & \\ \end{array}$ |
| $C^{16} - H^{17}$ 113.000 $C^{16} - H^{17}$ 106.957 $C^{16} - C^{14}$ 108.888 |
| C ¹⁶ -H ¹⁷ 106.957 C ¹⁶ -C ¹⁴ 108.888 |
| $C^{16} - C^{14}$ 108.888 |
| |
| C ¹⁶ - C ¹⁴ 109.292 |
| |
| C ¹⁴ - C ³ 112.923 |
| C14 - H15 108.459 |
| C ¹⁴ – H ²² 108.723 |
| C ¹⁴ - C ³ 109.390 |
| C14 - H15 106.931 |
| C ¹⁴ - C ³ 110.225 |
| C3 - C4 120.395 |
| C ³ – C ² 121.381 |
| C ⁴ – C ⁵ 120.885 |
| C ⁴ – H ⁹ 120.076 |
| C ⁴ - C ⁵ 119.039 |
| C ⁵ – C ⁶ 120.370 |
| C ⁵ – O ¹² 124.100 |
| D ¹² – H ¹³ 110.677 |
| C ⁵ – C ⁶ 115.530 |
| C ⁶ – O ¹⁰ 121.030 |
| C ⁶ - C ¹ 119.186 |
| D ¹⁰ – H ¹¹ 109.208 |
| |

| SI. No. | Bond | Bond length [Å] DFT/B3LYP/ 6-311++ g(d,p) | Bond | Bond Angle (°) DFT/B3LYP/ 6-311++g(d,p) |
|------------|-----------------------------------|---|---|---|
| 27 | C46 - C48 | 1.396 | $C^6 - C^1 - C^2$ | 120.234 |
| 28 | $C^{48} - H^{51}$ | 1.084 | $O^{10} - C^6 - C^1$ | 119.783 |
| 29 | $C^{48} - C^{44}$ | 1.394 | C6 - C1 - H7 | 118.840 |
| 30 | C44 - H49 | 1.084 | $C^1 - C^2 - C^3$ | 121.123 |
| 31 | $C^{44} - C^{42}$ | 1.394 | $H^7 - C^1 - C^2$ | 120.925 |
| 32 | C42 - H45 | 1.083 | $C^1 - C^2 - H^8$ | 119.184 |
| 33 | $C^{42} - C^{41}$ | 1.402 | $H^8 - C^2 - C^3$ | 119.692 |
| 34 | $C^{41} - C^{24}$ | 1.492 | $C^2 - C^3 - C^4$ | 118.202 |
| 35 | C ²⁴ = N ³³ | 1.284 | H ⁵⁰ - C ⁴⁶ - C ⁴³ | 119.773 |
| 36 | N ³³ - C ²³ | 1.458 | H ⁵⁰ - C ⁴⁶ - C ⁴⁸ | 120.060 |
| 37 | C ²³ - H ⁵³ | 1.098 | C ⁴⁶ - C ⁴³ - H ⁴⁷ | 120.440 |
| 38 | $C^{23} - H^{27}$ | 1.088 | C ⁴⁶ - C ⁴³ - C ⁴¹ | 120.526 |
| 39 | $C^{23} - C^{25}$ | 1.523 | $C^{43} - C^{41} - C^{24}$ | 119.847 |
| 40 | $C^{25} = O^{39}$ | 1.225 | C ⁴³ - C ⁴¹ - C ⁴² | 118.913 |
| 41 | $C^{25} - N^{34}$ | 1.377 | $C^{24} - C^{41} - C^{42}$ | 121.209 |
| 42 | N ³⁴ - C ³⁵ | 1.471 | C ⁴¹ - C ⁴² - H ⁴⁵ | 119.990 |
| 43 | $C^{35} - H^{38}$ | 1.088 | C ⁴¹ - C ⁴² - C ⁴⁴ | 120.489 |
| 44 | $C^{35} - H^{37}$ | 1.093 | H ⁴⁵ - C ⁴² - C ⁴⁴ | 119.513 |
| 45 | C ³⁵ – H ³⁶ | 1.088 | C ⁴² - C ⁴⁴ - C ⁴⁸ | 120.152 |
| 46 | N ³⁴ - C ²⁶ | 1.420 | C ⁴² - C ⁴⁴ - H ⁴⁹ | 119.701 |
| 47 | $C^{26} - C^{32}$ | 1.412 | H ⁴⁹ - C ⁴⁴ - C ⁴⁸ | 120.147 |
| 48 | $C^{32} - C^{24}$ | 1.489 | C ⁴⁴ - C ⁴⁸ - H ⁵¹ | 120.125 |
| 49 | $C^{32} - C^{31}$ | 1.404 | C ⁴⁴ - C ⁴⁸ - C ⁴⁶ | 119.748 |
| 50 | C31 - H55 | 1.082 | H ⁵¹ - C ⁴⁸ - C ⁴⁶ | 120.126 |
| 51 | $C_{31} = C_{30}$ | 1.383 | $C^{41} - C^{24} - C^{32}$ | 118.674 |

Table 1 (Part 1): Bond lengths and Bond angles of Optimized structure of Dopamine – Diazepam biomolecular complex.

3.2 Analysis of Natural Bond Orbitals (NBO)

The charge transfer mechanisms in organic compounds can be categorized into intramolecular and intermolecular charge transfer. The intra and intermolecular charge transfer behaviour of a compound can be analyzed using Natural Bond Orbital (NBO) analysis. NBO analysis, a well-established and comprehensive method, is based on solving the Schrödinger equation for multi-electron systems. Second-order perturbation theory is applied to examine charge transfer between donor (i) and acceptor (j) orbitals and to calculate their corresponding stabilization energies (E). The stabilization energy reflects the strength of the interaction, distinguishing between weak and strong interactions. Stabilization energy (E^2) associated with donor-acceptor delocalization $i \to j$ is calculated via the second-order Fock matrix [62, 63, 64].

$$E^{2}(q) = \Delta E_{ij} = q_{i} \frac{F(i,j)^{2}}{\epsilon_{i} - \epsilon_{i}}$$

$$\tag{1}$$

Where q_i stands for occupancy of donor orbital, ϵ_j and ϵ_i represent the components of diagonal, F(i,j) indicates diagonal NBO Fock matrix component, i and j are indices representing donors and acceptors orbital. The stabilization energy (E^2) of the donor and acceptor orbitals estimated using the equation provided for the Dopamine – Diazepam biomolecular complex is described in table S-2 in appendix A. In the Dopamine–Diazepam biomolecular complex, both lone pair and bond pair orbitals play pivotal roles in the complex's stability and charge transfer between the monomers. Significant energy transferred between Dopamine and Diazepam monomers is observed between $n_1({\rm O}^{12}) \to \sigma^*({\rm C}^{29}-{\rm H}^{54}), \, n_2({\rm O}^{12}) \to \sigma^*({\rm C}^{29}-{\rm H}^{54}), \, n_2({\rm Cl}^{40}) \to \sigma^*({\rm O}^{10}-{\rm H}^{11})$, and $n_3({\rm Cl}^{40}) \to \sigma^*({\rm O}^{10}-{\rm H}^{11})$ with 0.74 kJ/mol, 0.71 kJ/mol, 0.52 kJ/mol, and 0.29 kJ/mol, confirming the charge transfer with the formation of a hydrogen bond of the type $({\rm H}^{13}-{\rm O}^{12}-{\rm H}^{54})$ and $({\rm O}^{10}-{\rm H}^{11}-{\rm Cl}^{40})$ hydrogen bonding with weak interactions as energy is very low at 29 and 66 BCPs.



| SI. No. | Bond | Bond length [Å] DFT/B3LYP/ 6-311++ g(d,p) | Bond | Bond Angle (°) DFT/B3LYP/ 6-311++g(d,p) |
|------------|------------------------------------|---|---|---|
| 52 | C ³⁰ - Cl ⁴⁰ | 1.764 | $C^{24}-C^{32}-C^{31}$ | 118.858 |
| 53 | $C^{30}-C^{29}$ | 1.392 | $C^{32}-C^{31}-H^{55}$ | 119.524 |
| 54 | C ²⁹ - H ⁵⁴ | 1.082 | $C^{32} - C^{31} = C^{30}$ | 120.396 |
| 55 | $C^{29} - C^{28}$ | 1.387 | $C^{31} = C^{30} - C1^{40}$ | 119.306 |
| 56 | C ²⁸ - H ⁵² | 1.082 | $C_{31} = C_{30} - C_{50}$ | 121.174 |
| 57 | $C^{28} - C^{26}$ | 1.403 | C ³⁰ - C ²⁹ - H ⁵⁴ | 120.679 |
| 58 | H ¹¹ – Cl ⁴⁰ | 2.855 | $C^{30} - C^{29} - C^{28}$ | 118.814 |
| 59 | O ¹² - H ⁵⁴ | 2.533 | C ²⁹ - C ²⁸ - H ⁵² | 118.877 |
| 60 | | | $C^{29}-C^{28}-C^{26}$ | 121.401 |
| 61 | | | H ⁵² - C ²⁸ - C ²⁶ | 119.716 |
| 62 | | | $C^{28} - C^{26} - C^{32}$ | 119.186 |
| 63 | | | $C^{28} - C^{26} - N^{34}$ | 118.598 |
| 64 | | | $C^{26}-C^{32}-C^{31}$ | 119.007 |
| 65 | | | $C^{26}-C^{32}-C^{24}$ | 122.132 |
| 66 | | | C32 - C26 - N34 | 122.164 |
| 67 | | | $C^{26} - N^{34} - C^{25}$ | 123.003 |
| 68 | | | $C^{26} - N^{34} - C^{35}$ | 118.922 |
| 69 | | | $C^{35} - N^{34} - C^{25}$ | 117.292 |
| 70 | | | $N^{34} - C^{35} - H^{36}$ | 109.011 |
| 71 | | | $N^{34} - C^{35} - H^{38}$ | 108.384 |
| 72 | | | N ³⁴ - C ³⁵ - H ³⁷ | 111.770 |
| 73 | | | H ³⁶ - C ³⁵ - H ³⁷ | 109.622 |
| 74 | | | H ³⁶ - C ³⁵ - H ³⁸ | 109.554 |
| 75 | | | H ³⁷ - C ³⁵ - H ³⁸ | 108.468 |

| SL No. | Bond | Bond length [Å] DFT/B3LYP/ 6-311++ g(d,p) | Bond | Bond Angle (°) DFT/B3LYP/ 6-311++g(d,p) |
|-----------|------|---|--|---|
| 76 | | | $N^{34} - C^{25} = O^{39}$ | 121.933 |
| 77 | | | N ³⁴ - C ²⁵ - C ²³ | 115.590 |
| 79 | | | C ²⁵ - C ²³ - H ⁵³ | 109.663 |
| 80 | | | $C^{23} - N^{33} = C^{24}$ | 118.277 |
| 81 | | | H ²⁷ - C ²³ - N ³³ | 109.180 |
| 82 | | | H ⁵³ - C ²³ - N ³³ | 112.120 |
| 83 | | | $N^{33} = C^{24} - C^{41}$ | 117.926 |
| 84 | | | $N^{33} = C^{24} - C^{32}$ | 123.396 |
| 85 | | | $H_{22} - C_{21} = C_{30}$ | 120.080 |
| 86 | | | C ²⁹ - C ³⁰ - Cl ⁴⁰ | 119.519 |

Table 1(Part 2): Bond lengths and Bond angles of Optimized structure of Dopamine – Diazepam biomolecular complex.

The strong interactions are demonstrated by orbital interactions $\pi^*(C^5-C^6) \to \pi^*(C^3-C^4)$, $\pi(C^{29}-C^{30}) \to \pi^*(C^{31}-C^{32})$, $\pi(C^{26}-C^{28}) \to \pi^*(C^{31}-C^{32})$, $n_2(O^{10}) \to \pi^*(C^5-C^6)$, $n_2(O^{12}) \to \pi^*(C^5-C^6)$, $n_1(N^{19}) \to \sigma^*(C^{16}-H^{17})$, $n_1(N^{34}) \to \pi^*(C^{25}=O^{39})$, $n_2(O^{39}) \to \sigma^*(C^{25}-N^{34})$, and $n_3(C^{140}) \to \pi^*(C^{29}-C^{30})$ with strong stabilization energies of 196.83 kJ/mol, 83.36 kJ/mol, 93.19 kJ/mol, 26.04 kJ/mol, 20.34 kJ/mol, 7.33 kJ/mol, 56.51 kJ/mol, 26.13 kJ/mol, and 11.23 kJ/mol.

The highest stabilization energy score by the Dopamine – Diazepam biomolecular complex is 251.96 kJ/mol exhibited by the donor $\pi^*(C^5-C^6)$ and the acceptor $\pi^*(C^1-C^2)$. The higher stabilization energy displayed by the biomolecular complex suggests that there is substantial energy transfer with excellent donor-acceptor interaction, thereby significantly affecting the stability of the complex [65].

3.3 Molecular Electrostatic Potential (MEP) surface analysis

The Molecular Electrostatic Potential (MEP) map provides a three-dimensional visualization of the electron density distribution within a molecule. This tool is widely utilized to interpret and predict reactive sites and identify potential pathways for intermolecular hydrogen bonding interactions [66, 67, 68]. Figure 2 displays the computed MEP plots for the Dopamine–diazepam biomolecular complex. In MEP analysis, potential gradients are depicted using color coding: red represents regions of high electronegativity, blue indicates areas of high electropositivity, and green corresponds to neutral electrostatic potential [69, 70, 71, 72]. The variation in electric potential is such that nucleophilicity decreases in the order red > orange > yellow > green > blue [73]. The coexistence of electropositive and electronegative regions in the individual molecules supports the formation of the Dopamine - Diazepam complex via intermolecular hydrogen bonding. It is found that the red regions are primarily concentrated around the oxygen and the chlorine atoms, whereas the blue regions are mainly associated with the hydrogen atoms. Specifically, the complex exhibits hydrogen bonding between Dopamine and Diazepam at $(H^{13} - O^{12} \cdots H^{54})$ and $(O^{10} - H^{11} \cdots Cl^{40})$ with an isosurface value ranging from -0.141 a.u. to 0.141 a.u.



This highlights the pivotal role of oxygen, chlorine, and hydrogen atoms in facilitating charge transfer mechanisms, which are crucial for biological recognition processes.

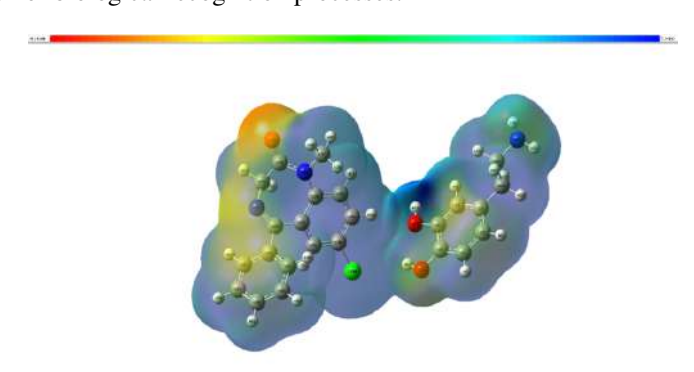


Figure 2: Molecular Electrostatic Potential map of Dopamine - Diazepam biomolecular complex.

3.4 Analysis of Frontier Molecular Orbital (FMO)

The highest occupied molecular orbital (HOMO) and the lowest unoccupied molecular orbital (LUMO), collectively referred to as Frontier Molecular Orbitals (FMOs), are essential for understanding a molecule's chemical reactivity and optical properties. HOMOs, being electron-rich, act as electron donors, while LUMOs, being electron-deficient, function as acceptors. The energies of the HOMO and LUMO, along with the energy gap ($E_{LUMO}-E_{HOMO}$) between them, are key factors influencing the molecule's reactivity and stability [74, 75]. The FMO of Dopamine –Diazepam biomolecular complex is depicted in figure 3. The computed frontier orbital gap for the biomolecular complex is found to be –2.51 eV, which is large, likely due to hydrogen bonding within the complex (table 2). This energy gap suggests enhanced charge transfer potential, resulting in increased bioactivity and decreased kinetic stability of the complex [76, 77]. Additionally, the HOMO and LUMO energies provide insights into quantum chemical parameters such as chemical hardness (η), chemical potential (μ), electron affinity (EA), ionization energy (IE), and the electrophilicity index (ω), which can be calculated using Koopmans' theorem [78]. Thus, FMO analysis is critical in molecular modeling and understanding molecular properties.

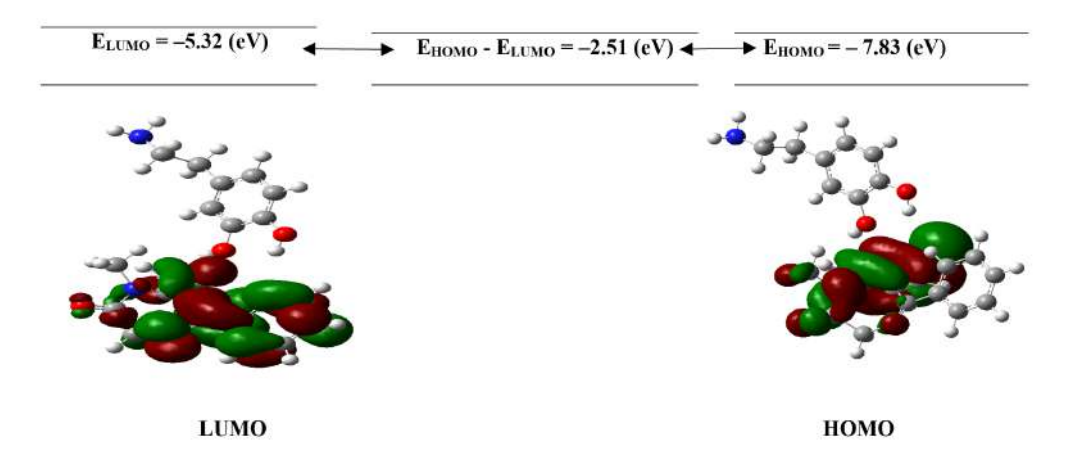


Figure 3: HOMO – LUMO energy gap of Dopamine – Diazepam biomolecular complex.

3.5 Analysis of Thermodynamic properties and quantum parameters

The study of thermodynamic properties, including Self-Consistent Field (SCF) energy, Zero-Point Vibrational Energy (ZPVE), total thermal energy, and rotational constants, is essential for understanding the energetic inter-



actions within molecular complexes. These parameters are determined using factors such as specific heat, statistical thermodynamic partition functions, entropy, enthalpy, and related properties. For the Dopamine–Diazepam biomolecular complex, these thermodynamic parameters are summarized in table 2. The analysis reveals that the Dopamine–Diazepam biomolecular complex exhibits higher SCF energy -1779.54 Hartree and total thermal energy 293.34 kcal mol^{-1} . Additionally, key properties such as the electrophilicity index (ω) , chemical potential (μ) , electron affinity (EA), ionization energy (IE), and chemical hardness (η) are highlighted in table 2. The combined electrophilicity index of the complex 17.32 is high, indicating enhanced electron transfer between donors and acceptors, along with a pronounced electrophilic character and improved bioactivity [79].

| Parameters | Dopamine – Diazepam | | |
|---|---------------------|--|--|
| SCF (Hartree) | - 1779.54 | | |
| Total thermal Energy (kcal mol ⁻¹) | 293.34 | | |
| Zero-point Vibrational Energy (kcal mol ⁻¹) | 274.55 | | |
| Rotational Constants (GHz) | | | |
| A | 0.21 | | |
| В | 0.05 | | |
| C | 0.04 | | |
| E_{LUMO} | -5.32(eV) | | |
| Еномо | -7.83(eV) | | |
| E _{HOMO} - E _{LUMO} | -2.51(eV) | | |
| Hardness (η) = $\frac{1}{2}$ (E _{LUMO} – E _{HOMO}) | 1.25(eV) | | |
| Chemical potential (μ) =½ ($E_{HOMO} + E_{LUMO}$) | -6.58(eV) | | |
| Electronegativity (χ) = -1/2 (E _{HOMO} + E _{LUMO}) | 6.58 (eV) | | |
| I.E. = - E _{HOMO} | 7.83(eV) | | |
| E.A. = - E _{LUMO} | 5.32(eV) | | |
| Global electrophilicity index $(\omega) = \!$ | 17.32 | | |
| | | | |

Table 2: Thermodynamic and quantum chemical parameters of Dopamine – Diazepam biomolecular complex to examine chemical reactivity and stability.

The significant negative value of the complex's chemical potential – 6.58 eV implies resistance to rapid decomposition and lower reactivity [80]. Chemical hardness (η), a measure of resistance to charge transfer, decreases as the energy gap narrows in the complex, suggesting increased polarizability and heightened reactivity. Conversely, chemical softness, the reciprocal of hardness, reflects the ease of electron density transfer, supporting the enhanced stability and binding of the complex [81]. The electron affinity, which represents the energy released when an electron attaches to a neutral species, is positive for the complex with 5.32 eV, indicating exothermic electron capture. Similarly, ionization energy, reflecting the energy required to remove an electron, is slightly lower for the complex, suggesting that the complex is marginally more reactive [82, 83]. The zero-point vibrational energy of the Dopamine–Diazepam complex is 274.55 kcal mol^{-1} further suggests increased reactivity [84]. This underscores the strong binding and stability of the Dopamine–Diazepam complex, driven by the active participation of the monomers in their interactions.



3.6 Analysis of Nonlinear optical (NLO) properties

In recent decades, researchers have paid significant attention to nonlinear optical (NLO) materials due to their diverse applications in image processing, frequency shifting, all-optical switching, and image manipulation. For a system to exhibit active NLO properties, it must possess high hyperpolarizability and dipole moment values. It is well-established that systems with narrow frontier orbital gaps tend to demonstrate enhanced hyperpolarizability, contributing to strong nonlinear optical characteristics. The Dopamine–Diazepam biomolecular complex, with a reduced energy gap of -2.51 eV (table 2), indicates potential NLO activity. This potential is typically assessed by calculating the first-order hyperpolarizability (FOHP), a rank-3 tensor initially consisting of 27 components, which are reduced to ten by applying Kleinman symmetry. FOHP is not only crucial for evaluating NLO properties but also plays an important role in drug design and pharmaceutical applications [85, 86, 87]. In this study, the dipole moment and first-order hyperpolarizability of the complex were computed. The FOHP, calculated using equation (2), provides further insights into the NLO behavior of the system.

$$\beta_{\text{tot}} = (\beta_x^2 + \beta_y^2 + \beta_z^2)^{1/2} \tag{2}$$

where

$$\beta_x = \beta_{xxx} + \beta_{xyy} + \beta_{xzz}, \ \beta_y = \beta_{yyy} + \beta_{yzz} + \beta_{yxx}, \ \beta_z = \beta_{zzz} + \beta_{zxx} + \beta_{zyy}$$

and β_{tot} indicates the total hyperpolarizability. On the other hand, μ , defined as

$$\mu = (\mu_x^2 + \mu_y^2 + \mu_z^2)^{1/2} \tag{3}$$

represents the total dipole moment, with its components along the x,y and z axes denoted as μ_x , μ_y , and μ_z , respectively. The total first-order hyperpolarizability is represented by β_{tot} . The computed hyperpolarizability values, initially in atomic units, are converted to electrostatic units (esu) using the conversion factor 1 a.u. = 8.639×10^{-33} esu. As shown in table 3, the β_{tot} value for the Dopamine–Diazepam complex is 3.260×10^{-30} esu—approximately 16 times higher than the threshold value of urea $(0.1947 \times 10^{-30} \text{ esu})$, a standard reference molecule for NLO studies [88]. The dipole moments of the complex are determined to be 5.19 Debye, respectively (table 3). The significantly elevated dipole moment and first-order hyperpolarizability of the complex indicate a higher degree of electron density transfer from donor to acceptor moieties, which aligns with the reduced frontier orbital gap of the biomolecular complex [89]. As the energy gap narrows, maximal electron transfer occurs between the donor and acceptor, enhancing both the hyperpolarizability and dipole moment in the interacting state. This increase in β and μ is attributed to intermolecular hydrogen bonding between Dopamine and Diazepam, which amplifies the NLO activity of the complex [90].

3.7 Drug-likeness Analysis

The concept of drug-likeness plays a vital role in the early stages of drug discovery, evaluating a compound's potential as a therapeutic agent. Drug-likeness encompasses a range of physicochemical properties, such as molecular weight, hydrogen bond acceptors and donors, total polar surface area (TPSA), and the number of rotatable bonds, all of which influence a drug's oral bioavailability. Parameters like MilogP and logP are also critical for assessing molecular hydrophobicity, which affects drug toxicity, bioavailability, and receptor interactions [91]. A greater number of rotatable bonds often correlates with enhanced binding affinity and molecular flexibility [92]. TPSA is particularly useful for predicting blood-brain barrier (BBB) penetration, intestinal absorption, and membrane permeability. Drug-likeness evaluation commonly follows Lipinski's rule of five, which suggests that for optimal membrane permeability, a molecule should have a molecular weight below 500 daltons, a logP value not exceeding 5, no more than 5 hydrogen bond donors, and no more than 10 hydrogen bond acceptors [93]. Table 4 summarizes the drug-likeness parameters for the biomolecular complex. The TPSA value for the complex is 99.15 Å², respectively. The biomolecular complex exhibits a molecular weight of 437.92 g/mol, MilogP of 2.27, 3 hydrogen bond donors, 5 hydrogen bond acceptors, and 3 rotatable bonds. These findings indicate that the biomolecular complex adheres well to Lipinski's criteria, suggesting good oral bioavailability and significant pharmacological potential.

3.8 Analysis of Atoms in Molecule (AIM)

AIM (Atoms in Molecules) analysis, based on electron density (ρ) at bond critical points (BCPs) and the Laplacian of electron density ($\nabla^2 \rho_{\rm BCP}$), provides insights into the nature of intermolecular bonding and the existence of



| Parameters | Dopamine – Diazepam | |
|--------------------|-------------------------------|--|
| β_{xxx} | - 126.6468 | |
| _{Бууу} | -91.9286 | |
| β_{zzz} | 19.4045 | |
| β_{xyy} | - 81.5229 | |
| β _{xxy} | -155.9980 | |
| β_{xxz} | -95,2271 | |
| β_{xzz} | -65.7331 | |
| β _{yzz} | 8.2928 | |
| β _{ууz} | -24.2590 | |
| β _{total} | 377.44 a.u. | |
| | = 3.260×10 ⁻³⁰ esu | |
| Dipole moment | 5.19 Debye | |
| | | |

Table 3: First-order hyperpolarizability and dipole moment of Dopamine – Diazepam biomolecular complex.

| ligand | TPSA (Ų) | Molecular weight(g/mol) | Milog P | Hydrogen bond donors | Hydrogen bond acceptors | Number of rotatable bonds |
|------------------------|-------------|----------------------------|---------|-------------------------|-------------------------|---------------------------|
| Dopamine – Diazepam | 99.15 | 437.92 | 2.27 | 3 | 5 | 3 |

Table 4: Physicochemical properties of Dopamine – Diazepam biomolecular complex.

hydrogen bonds [94]. A high $\rho(r)$ value with $\nabla^2\rho(r)<0$ indicates polar or nonpolar covalent bonds, whereas a low $\rho(r)$ value and $\nabla^2\rho(r)>0$ suggest closed-shell interactions [95]. Hydrogen bonds can be classified into three categories based on $\nabla^2\rho_{\rm BCP}$ and $H_{\rm BCP}$ values: strong hydrogen bonds with covalent characteristics ($\nabla^2\rho_{\rm BCP}<0$, $H_{\rm BCP}<0$), medium hydrogen bonds with partial covalent nature ($\nabla^2\rho_{\rm BCP}>0$, $H_{\rm BCP}<0$), and weak hydrogen bonds with electrostatic interactions ($\nabla^2\rho_{\rm BCP}>0$, $H_{\rm BCP}>0$) [96,97]. The electron density of $H_{\rm BCP}$ at BCPs further characterizes the nature of hydrogen bonding [98]. According to Koch and Popelier, hydrogen bonds can be confirmed if $\rho(r)$ lies between 0.002 and 0.040 a.u., $\nabla^2\rho(r)$ is positive and ranges from 0.024 to 0.139 a.u., and a BCP is present [99]. In this study, bond critical points for the Dopamine–Diazepam complex are identified at BCP 29 and 66, with critical points [3, -1]. At BCP 29, the hydrogen bond ($H^{13}-O^{12}-H^{54}$) has $\nabla^2\rho_{\rm BCP}$ and $H_{\rm BCP}$ values of -0.7425 and -1.8620, suggesting strong hydrogen bonds with covalent characteristics, while at BCP 66, the bond ($O^{10}-H^{11}-Cl^{40}$) shows $\nabla^2\rho_{\rm BCP}$ and $H_{\rm BCP}$ values of 0.0211 and



0.0014 depicting weak hydrogen bonds with electrostatic characteristics (table 5). Covalent bonding interactions typically exhibit $\rho(r)>0.20$ a.u., while closed-shell interactions show $\rho(r)<0.10$ a.u. A positive $\nabla^2\rho$ suggests electrostatic bonding, with electron density decreasing along the bond path, while a negative $\nabla^2\rho$ indicates a covalent nature, with electron density concentrated near the nuclei. The energy density H(r), determined as the sum of Lagrangian kinetic energy G(r) and potential energy density V(r), further reflects bonding stability. A positive H(r) denotes unstable charge density, whereas a negative H(r) indicates stabilization at the BCP, characteristic of covalent bonding.

| Hydrogen Bonds | DFT | | | | | | |
|--|--------|------------------------|---------|---------|----------|------|--|
| | рвсрѕ | $\nabla^2 \rho_{BCPS}$ | H(r) | G(r) | V(r) | Eint | |
| H ¹³ – O ¹² – H ⁵⁴ | 0.3537 | - 0.7425 | -1.8620 | -0.0055 | - 0.0061 | 1.91 | |
| O ¹⁰ – H ¹¹ – Cl ⁴⁰ | 0.0055 | 0.0211 | 0.0014 | 0.0039 | - 0.0025 | 0.78 | |

Table 5: The electron density (ρ) , the Laplacian of electron density $(\nabla^2 \rho)$, the energy density (H(r)), Lagrangian K.E. (G(r)), potential energy density (V(r)), and inter-atomic interaction energies $(E_{\rm int})$ at the bond critical points (BCPs) of Dopamine – Diazepam biomolecular complex.

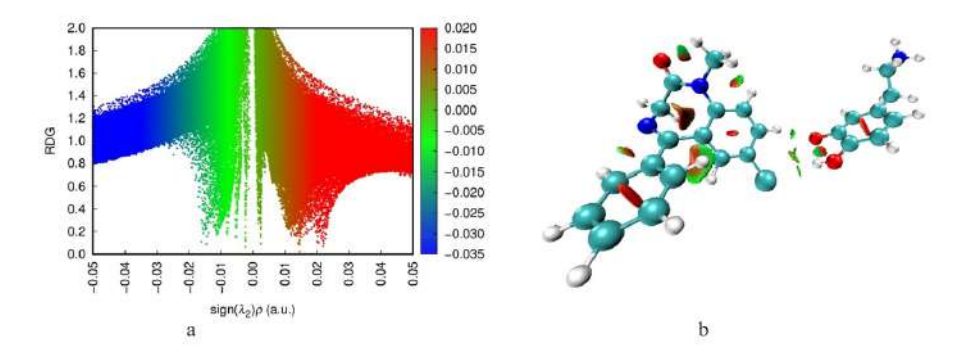


Figure 4: Dopamine–Diazepam biomolecular complex's (a) 2D scatter map (b) NCI iso-surface HOMO – LUMO energy gap of Dopamine – Diazepam biomolecular complex

The interatomic interaction energies (E_{int}) of the biomolecular complex given by,

$$E_{\text{int}}(\text{a.u.}) = -\frac{1}{2}V(r) \times 625.51$$
 (4)

were also evaluated using the Espinosa approach, offering insights into bonding strength and interactions [100]. The $E_{\rm int}$ values for the hydrogen bonds in the Dopamine–Diazepam biomolecular complex, contributed by (H¹³–O¹² – H⁵⁴) and (O¹⁰ – H¹¹ – Cl⁴⁰) are calculated as 1.91 kcal mol⁻¹ and 0.78 kcal mol⁻¹, respectively (table 5). These findings indicate that the noncovalent interactions within the biomolecular complex are weak and predominantly governed by van der Waals forces.

3.9 Non – Covalent Interaction (NCI) Analysis

Noncovalent Interaction (NCI) analysis is valuable for investigating various interactions, including steric effects, hydrogen bonding, van der Waals forces, and hydrophobic interactions. While NCI primarily employs a topological approach based on electron density, it also facilitates the characterization of noncovalent bonds. These interactions are classified using a scalar function and a dimensionless parameter known as the reduced density



gradient (RDG). RDG, represented as S(r), can be calculated at any point in three-dimensional space using the electron density (ρ) and its first derivative $(\nabla \rho)$ as [101]

$$S(r) = \frac{1}{2(3\pi)^{1/3}} \frac{|\nabla \rho|}{\rho^{4/3}}.$$
 (5)

The nature of the interaction, whether attractive or repulsive, is determined by analyzing the electron density in the Hessian matrix and the second eigenvalue (λ_2). A positive λ_2 indicates repulsive interactions, such as steric repulsion, while a negative λ_2 suggests attractive interactions, like hydrogen bonds [102]. When λ_2 approaches zero, it signifies van der Waals interactions. NCI isosurfaces, generated using VMD 1.9.2 software, help visualize these interactions based on the reduced density gradient (RDG) [103]. These isosurfaces represent different types of interactions with distinct colors: blue indicates attractive interactions such as hydrogen bonds and halogen bonds, green represents fragile interactions like van der Waals forces, and red denotes steric repulsions. The 2D scatter map for the Dopamine-Diazepam biomolecular complex, shown in left panel of figure 4, reveals significant negative peaks, indicating intermolecular attractive interactions, along with positive peaks corresponding to steric effects. Additionally, the presence of van der Waals interactions is confirmed by peaks between these extremes. Interaction critical points (ICP) are inferred from these scatter map peaks, helping to assess the strength of noncovalent interactions [104]. Stronger attractive ($\lambda_2 < 0$) or repulsive ($\lambda_2 > 0$) interactions are indicated by higher electron density at the ICPs [105]. Regions with $sign(\lambda_2)\rho(r) > 0.05$ a.u. on the scatter map suggest strong steric repulsions, often related to nonbonded overlaps at ring centers. Specifically, the NCI isosurface is shown in right panel of figure 4 for the Dopamine-Diazepam biomolecular complex, highlighting strong hydrogen bonds, represented by blue-colored disk isosurfaces with negative eigenvalues ($\lambda_2 < 0$). Weak conventional hydrogen bonds and dihydrogen bonds are depicted by light blue and blue-green NCI isosurfaces, respectively. Red-colored critical points further illustrate the presence of dihydrogen bonds within a disk-like structure. Regions of the Dopamine–Diazepam complex with $\lambda_2 \simeq 0$ (either positive or negative) in the NCI isosurfaces correspond to van der Waals interactions, particularly dispersion forces, that contribute to complex binding at low electron densities. Small red rings around blue discs indicate electron density depletion due to electrostatic repulsion, representing the coordination sphere around the central atom.

3.10 Toxicity analysis

The toxicity evaluation of the Dopamine–Diazepam biomolecular complex was conducted using ProTox II, an *in silico* oral toxicity prediction platform. Drwal *et al.* performed a comprehensive *in silico* analysis assessing various toxicity parameters, including oral acute toxicity (median lethal dosage, LD₅₀, in mg/kg) and organ toxicity, focusing on hepatotoxicity, immunotoxicity, and genetic toxicity. The analysis also included endpoints such as cytotoxicity, mutagenicity, carcinogenicity, nuclear receptor signaling, and stress response pathways, including AhR, AR, AR-LBD, ER, and ER-LBD, molecular initiating events, and metabolism [106]. ProTox II is a freely accessible tool designed for toxicologists, regulatory agencies, and chemists to predict *in silico* toxicity [107]. The evaluation also included 2D structural similarities, identification of hazardous fragments, and classification into hazard classes I–VI based on the globally harmonized chemical labeling system [108]. Drwal *et al.* categorized substances based on toxicity levels: Class I (LD₅₀ \leq 5), Class II (5 < LD₅₀ \leq 50), Class III (50 < LD₅₀ \leq 300), Class IV (300 < LD₅₀ \leq 2000), Class V (2000 < LD₅₀ \leq 5000), and Class VI (LD₅₀ > 5000). The synthesized biomolecular complex was predicted to belong to Class IV (table 6a). Interestingly, combining Diazepam with Dopamine reduced its toxicity. ProTox II predicted LD₅₀ value for the biomolecular complex is 670 mg/kg, with graphical accuracy scores of 70.97%. The computed average structural similarity value is 85.42%.

The organ toxicity assessment revealed that the Dopamine–Diazepam biomolecular complex is active for neurotoxicity, clinical toxicity, and cytotoxicity with probability scores of 0.84, 0.67, and 0.52, respectively (table 6b). The biomolecular complex, nuclear receptor signaling, stress response pathways, molecular initiating events, and metabolism are all inactive. Nuclear receptor signaling pathways, including AhR, AR, AR-LBD, Aro, and ER, showed likelihood scores of 0.81, 0.95, 0.98, 0.92, and 0.89, while stress response pathways such as HSE and MMP had likelihood scores of 0.94 and 0.84. Molecular initiating events such as GABAR, THR α and THR β have scores of 0.62, 0.84, and 0.84, respectively. Metabolism such as CYP1A2 and CYP2C19 have scores of 0.81 and 0.75. Probability scores below 1 indicated a low likelihood of toxic effects, suggesting the compound's safety for human use [109]. Graphical representations of oral toxicity and predicted dosages confirmed the absence of toxic effects (figure 5).



Distribution of dose value

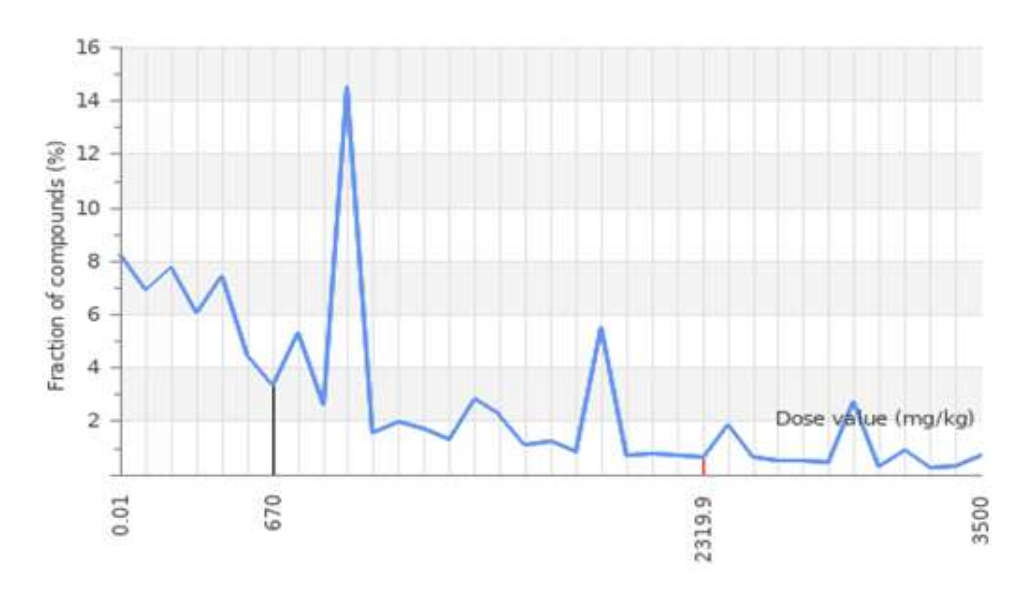


Figure 5: Graphical presentation of the oral toxicity of the predicted dose value of the Dopamine – Diazepam biomolecular complex

| | Dopamine – Diazepam |
|------------------------------------|---------------------|
| Predicted LD ₅₀ (mg/Kg) | 670 |
| Toxicity class | 4 |
| Average similarity (%) | 85.42 |
| Accuracy (%) | 70.97 |

Table 6a: Prediction of oral acute toxicity, class, average similarity, and prediction accuracy of Dopamine – Diazepam biomolecular complex

3.11 Theoretical and Experimental Vibrational Analysis

The molecular structure and functional groups influence the vibrational spectra of a molecule. Vibrational assignments are crucial for understanding interaction processes within a complex. Theoretical vibrational assignments for the Dopamine–Diazepam complex, calculated are provided in table 7. Theoretical and experimental FTIR and Raman spectra of the Dopamine–Diazepam biomolecular complex are presented in figure 6.

3.11.1 C- H stretching

C–H vibrational stretching typically occurs in the range of $2800-3000~\rm cm^{-1}$ [110, 111]. The computed C–H stretching for the biomolecular complex is observed at $2947~\rm cm^{-1}$ with a TED impact of 32% (table 7). The Dopamine–Diazepam complex exhibited its theoretical FTIR and Raman spectra for the C–H modes at $2942~\rm and$ $2902~\rm cm^{-1}$ (figure 6b and figure 6d). The experimental FTIR and Raman of the Dopamine–Diazepam complex exhibit this mode at $2935~\rm cm^{-1}$ and $2985~\rm cm^{-1}$ (figure 6b and figure 6d). It is found that the (C⁷–H³²) bond length remains constant, and therefore vibrational frequency is neither blueshifted nor redshifted.



| Classification | Target | Shorthand | Prediction | Probability |
|---|---|---------------|------------|-------------|
| Organ toxicity | Neurotoxicity | neuro | Active | 0.84 |
| Toxicity end points | Carcinogenicity | carcino | Inctive | 0.80 |
| Toxicity end points | Immunotoxicity | Immuno | Inactive | 0.86 |
| Toxicity end points | Clinical toxicity | mutagen | Active | 0.67 |
| Toxicity end points | Cytotoxicity | Cyto | Active | 0.52 |
| Tox21-Nuclear receptor signaling pathways | Aryl hydrocarbon Receptor (AhR) | nr_ahr | Inactive | 0.81 |
| Tox21-Nuclear receptor signaling pathways | Androgen Receptor (AR) | nr_ar | Inactive | 0.95 |
| Tox21-Nuclear receptor signaling pathways | Androgen Receptor Ligand Binding Domain (AR- LBD) | nr_ar_lbd | Inactive | 0.98 |
| Tox21-Nuclear receptor signaling pathways | Aromatase | nr_ aromatase | Inactive | 0.92 |
| Tox21-Nuclear receptor signaling pathways | Estrogen Receptor Alpha (ER) | nr_er | Inactive | 0.89 |
| Molecular initiating events | Thyroid hormone receptor alpha (THRα) | mie_thr_alpha | Inactive | 0.84 |
| Molecular initiating events | GABA receptor (GABAR) | mie_gabar | Inactive | 0.62 |
| Molecular initiating events | Thyroid hormone receptor beta (THR _β) | mie_thr_beta | Inactive | 0.84 |
| Tox21-Stress response pathways | Heat shock factor response element (HSE) | sr_hse | Inactive | 0.94 |
| Tox21-Stress response pathways | Mitochondrial Membrane Potential (MMP) | sr_mmp | Inactive | 0.84 |
| Metabolism | Cytochrome CYP1A2 | CYP1A2 | Inactive | 0.81 |
| Metabolism | Cytochrome CYP2C19 | CYP1A2 | Inactive | 0.75 |

Table 6b: Prediction of organ toxicity, toxicity endpoints, Tox21 - Nuclear receptor signaling pathways, Tox 21 - Stress response pathways, Molecular initiating events, and Metabolism of Dopamine - Diazepam biomolecular complex

3.11.2 N-H stretching

The N–H stretching mode typically occurs in the range of 3000–3500 cm⁻¹ [112]. The computed N–H stretching for the biomolecular complex is located at 3450 cm⁻¹ with 70% TED impact (table 7). Theoretical FTIR and Raman spectra for N–H vibrational modes are found at 3084 cm⁻¹ and 3088 cm⁻¹ (figure 6b and figure 6d). Experimentally, these modes are observed at 3433 cm⁻¹ and 3472 cm⁻¹ respectively (figure 6b and figure 6d). The (N¹⁹–H²⁰) bond exhibits a blueshift when comparing Dopamine to its biomolecular complex. This blueshift arises due to hydrogen bonding, causing a compression of the bond length from 1.016 Å in the monomer to 1.015 Å, resulting in the reduction of the bond's force constant. This leads to an increase in its vibrational frequency,



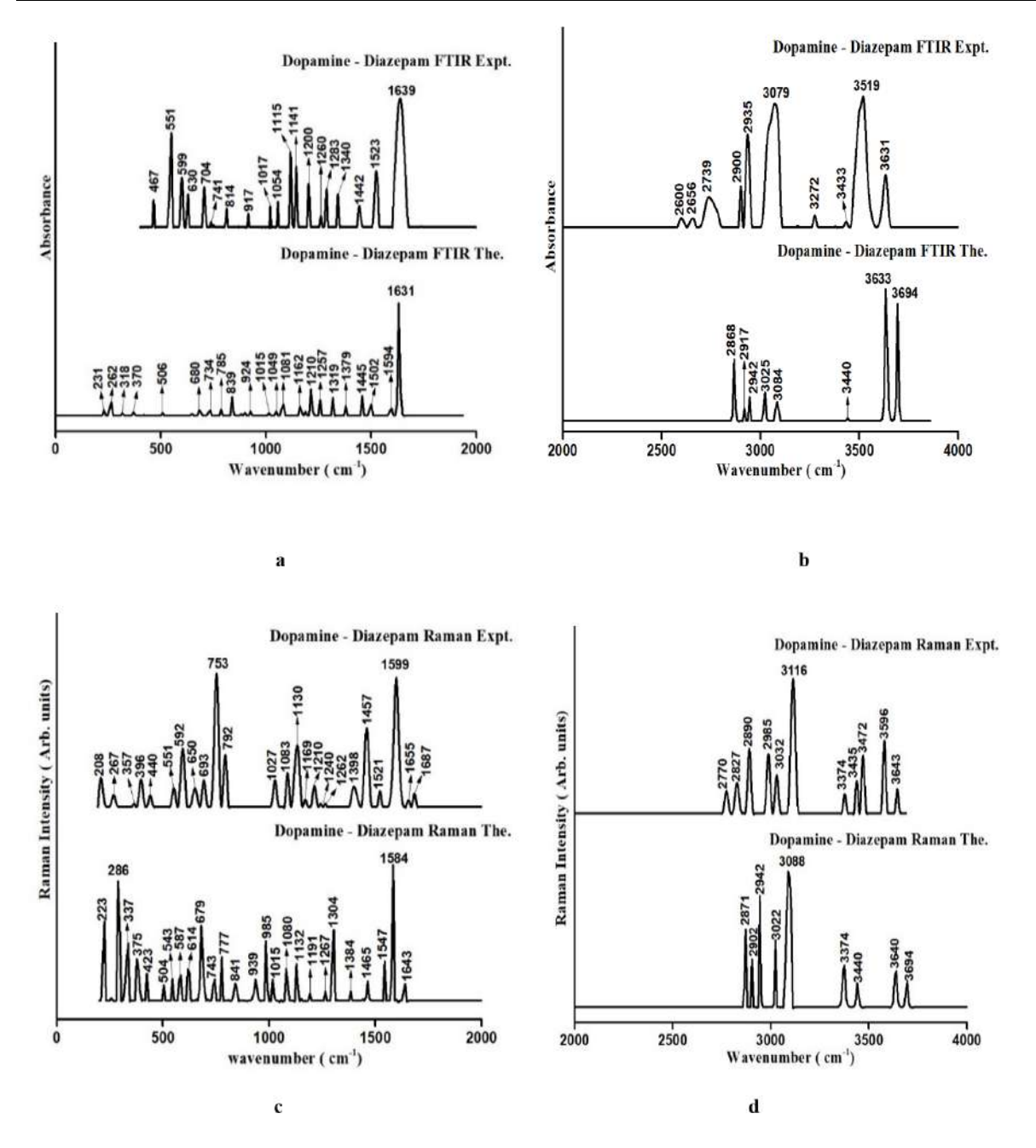


Figure 6: Dopamine–Diazepam biomolecular complex's (a) Theoretical and Experimental FTIR spectra in the range 0– $2000~cm^{-1}$ (b) Theoretical and Experimental FTIR spectra in the range 2000– $4000~cm^{-1}$ (c) Theoretical and Experimental Raman spectra in the range 2000– $4000~cm^{-1}$ (d) Theoretical and Experimental Raman spectra in the range 2000– $4000~cm^{-1}$

from $3310~{\rm cm^{-1}}$ to $3380~{\rm cm^{-1}}$, thereby confirming the presence of intermolecular hydrogen bonding in the biomolecular complex (table S-3a in appendix A and table 7).

3.11.3 C=O stretching vibration

A literature review indicates that the C=O carboxyl group typically exhibits stretching vibrations in the range of 1550–1850 cm⁻¹ [113]. The biomolecular complex displays computed C=O stretching vibrations at 1655 cm⁻¹ with 31% TED impact (table 7). The theoretical FTIR and Raman spectra for the Dopamine–Diazepam



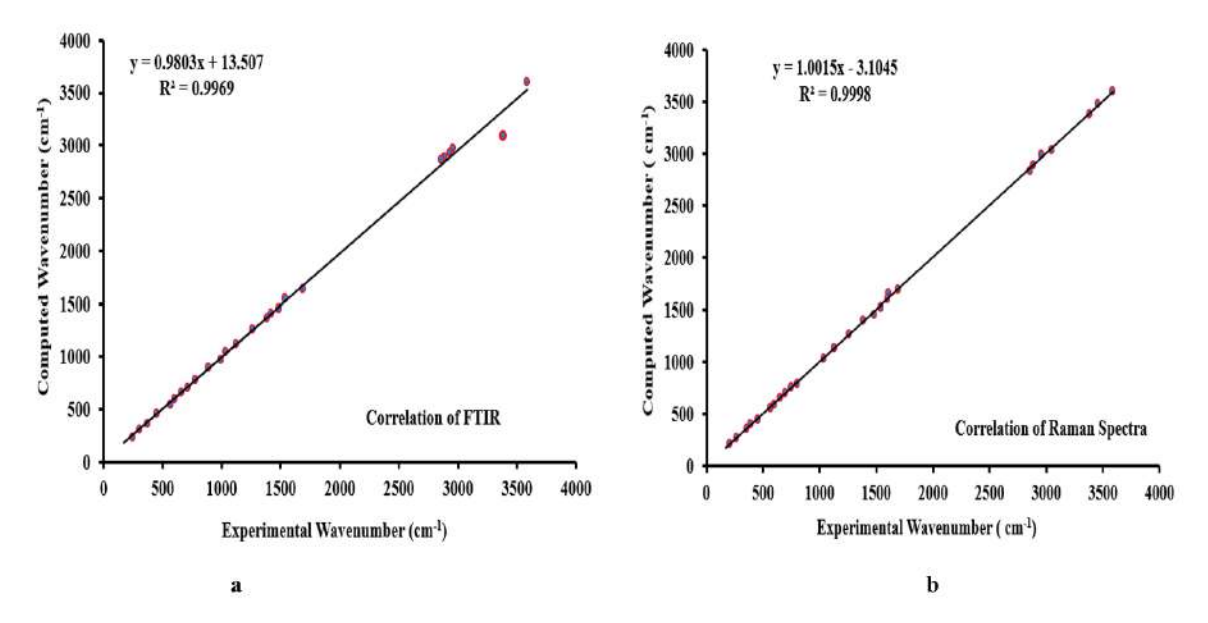


Figure 7: Correlation coefficient curve of Dopamine - Diazepam biomolecular complex (a) FTIR (b) Raman.

biomolecular complex appear at $1631~\rm cm^{-1}$ and $1584~\rm cm^{-1}$, while experimental bands are located at $1639~\rm cm^{-1}$ and $1599~\rm cm^{-1}$, respectively (figure 6a and figure 6c). The ($C^{25}=O^{39}$) bond displays a redshift when Diazepam is compared with its biomolecular complex. This redshift is caused by hydrogen bonding, which weakens the (C=O) bond and leads to an increase in the ($C^{25}=O^{39}$) bond length, from 1.214 Å in the monomer to 1.225 Å in the complex. The elongation lowers the bond's force constant, resulting in a reduction in its vibrational frequency from $1664~\rm cm^{-1}$ to $1655~\rm cm^{-1}$ (table S-3b in appendix A and table 7).

3.11.4 O-H stretching

The O–H functional group typically exhibits vibrational frequencies in the $3450-3600~\rm cm^{-1}$ range, as reported in the literature [114]. The Dopamine–Diazepam biomolecular complex displays O–H stretching at $3586~\rm cm^{-1}$ with a TED impact of 70% (table 7). Theoretical FTIR and Raman spectra for the Dopamine–Diazepam biomolecular complex show O–H stretching at $3633~\rm cm^{-1}$ and $3643~\rm cm^{-1}$. In comparison, experimental peaks appear at $3519~\rm cm^{-1}$ and $3596~\rm cm^{-1}$, respectively (figure 6b and figure 6d). When Dopamine is compared to its biomolecular complex, the $(O^{10}-H^{11})$ bond shows a redshift. This shift arises from hydrogen bonding, which weakens the O–H bond and elongates the $(O^{10}-H^{11})$ bond length from $0.966~\rm \AA$ in the monomer to $0.968~\rm \AA$ in the complex. The increased bond length reduces the force constant, decreasing its vibrational frequency from $3589~\rm cm^{-1}$ to $3586~\rm cm^{-1}$ (table S-3a in appendix A and table 7).

3.11.5 C-Cl stretching

The C–Cl functional group is commonly observed to exhibit vibrational frequencies near the 730 cm⁻¹ range, as documented in the literature [115]. For the Dopamine–Diazepam biomolecular complex, C–Cl stretching is identified at 742 cm⁻¹ with a TED contribution of 50% (table 7). Theoretical FTIR and Raman spectra predict C–Cl stretching at 734 cm⁻¹ and 743 cm⁻¹, respectively. In contrast, the experimental spectra display corresponding peaks at 741 cm⁻¹ and 753 cm⁻¹ (figure 6b and figure 6d). A redshift is observed in the (C³⁰–Cl⁴⁰) bond when Diazepam is compared to its biomolecular complex. This redshift results from hydrogen bonding (O¹⁰–H¹¹ ··· Cl⁴⁰), which weakens the C–Cl bond and extends its length from 1.757 Å in the monomer to 1.764 Å in the complex. The increase in bond length lowers the bond's force constant, thereby reducing its vibrational frequency from 782 cm⁻¹ to 742 cm⁻¹ (table S-3b in appendix A and table 7). It is also observed that there is charge transfer from $n_2(\text{Cl}^{40})$ to $\sigma^*(\text{O}^{10}-\text{H}^{11})$ in the NBO analysis (table S-2 in appendix A).

A correlation analysis between computed and experimental spectral data for the biomolecular complex reveals excellent agreement, with correlation coefficient values of 0.9969 for FTIR and 0.9998 for Raman spectra (figure



| Mode | Raman Expt. | FTIR Expt. | Scaled Wavenumber | Vibrational Assignments |
|------|----------------|------------|----------------------|--|
| 1 | 3596 | 3519 | 3586 | υ(O ¹⁰ – H ¹¹)70 |
| 2 | 3472 | 3433 | 3450 | $\upsilon(N^{19} - H^{20})70$, $\upsilon(N^{19} - H^{21})48$, $\beta(H^{18} - H^{20})$ |
| | • | | | $C^{16} - H^{17}$)11, $\tau(H^{18} - C^{16} - N^{19} - H^{21})$ 14 |
| 3 | 3374 | | 3380 | $\upsilon(N^{19}-H^{20})60$, $\upsilon(N^{19}-H^{21})44$, |
| 4 | | 3272 | 3272 | $υ(C^2 - H^8)47$, $β(H^8 - C^2 - C^1)13$, $τ(H^8 - C^2 - C^1)13$ |
| 5 | 3116 | | 3109 | $\upsilon(O^{12}-H^{13})29,\ \beta(H^{13}-O^{12}-H^{54})14,\ \tau(H^{13}-O^{12}-H^{54})14$ |
| 6 | | 3079 | 3075 | $\beta(H^{11}-O^{10}-C^6)16$, $\tau(H^{11}-O^{10}-C^6-C^6)$ |
| 7 | 3032 | | 3037 | $υ(O^{10} - H^{11})30$, $β(H^{18} - C^{16} - H^{17})28$, $β(H^{53} - C^{23} - H^{27})28$ |
| 8 | 2985 | | 2981 | $υ(C^{16} - H^{17})48$, $β(H^{13} - O^{12} - H^{54})37$, $τ(H^{15} - C^{14} - C^3 - C^2)13$, $β(H^{15} - C^{14} - H^{22})36$ |
| 9 | | | 2962 | $\beta(H^{13} - O^{12} - H^{54})24, \beta(H^{20} - N^{19} - H^{21})21,$ $\tau(H^{13} - O^{12} - H^{54} - C^{29})13$ |
| 10 | | | 2961 | $υ(O^{12} - H^{13})33$, $υ(C^{16} - H^{17})11$, $τ(H^{13} - O^{12} - H^{54} - C^{29})16$ |
| 11 | | 2935 | 2947 | $\upsilon(C^{16} - H^{17})32, \upsilon(C^{14} - H^{15})18,$ |
| 12 | | 2900 | 2936 | $\beta(H^9 - C^4 - C^5)22$, $\beta(H^{52} - C^{28} - C^{29})22$, $\beta(C^{29} - H^{54} - O^{12})22$, $\beta(H^{15} - C^{14} - H^{22})10$, $\tau(H^{18} - C^{16} - N^{19} - H^{21})12$ |
| 13 | | | 2916 | $β(H^9 - C^4 - C^5)29$, $β(H^{52} - C^{28} - C^{29})29$, $β(C^{29} - H^{54} - O^{12})29$, $τ(H^{18} - C^{16} - N^{19} - H^{21})13$ |
| 14 | 2890 | | 2868 | $υ(C^{14} - H^{15})38$, $β(H^{17} - C^{16} - N^{19})14$, $τ(H^9 - C^4 - C^5 - O^{12})16$ |
| 15 | 2827 | | 2826 | $\beta(H^7 - C^1 - C^6)39$, $\beta(H^9 - C^4 - C^5)15$, $\beta(H^{52} - C^{28} - C^{29})15$, $\beta(C^{29} - H^{54} - O^{12})15$ |
| 16 | 2770 | | 2794 | $\upsilon(C^1 - H^7)34$, $\tau(H^{15} - C^{14} - C^3 - C^2)24$ |
| 17 | | 2739 | 2707 | $υ(C^1 - H^7)10$, $β(H^7 - C^1 - C^6)26$ |
| 18 | | 2656 | 2651 | $\upsilon(C^4 - H^9)42$, $\tau(H^{15} - C^{14} - C^3 - C^2)16$, |
| 19 | | 2600 | 2546 | $\upsilon(C^1 - H^7)19$, $\upsilon(C^2 - H^8)11$, $\tau(H^7 - C^1 - C^6 - C^5)14$, $\tau(H^9 - C^4 - C^5 - O^{12})11$ |
| 20 | | | 2177 | $\beta(H^{36}-C^{35}-H^{38})28,\beta(H^{37}-C^{35}-H^{36})23,\\ \beta(H^{54}-O^{12}-C^{5})23,\tau(H^{36}-C^{35}-N^{34}-C^{25})17$ |

Table 7 (Part 1): ν – stretching; τ – torsion; β – in-plane bending; γ – out-of-plane bending; Theoretical and experimental wavenumbers (cm $^{-1}$) and potential energy distribution for vibrational modes of Dopamine–Diazepam biomolecular complex to understand the type of vibrations for identifying the compositions.

7a and figure 7b).

3.12 X-ray diffraction analysis

The crystalline behavior of the Dopamine–Diazepam biomolecular complex was analyzed using powder X-ray diffraction [116]. Data obtained from an X'pert Pro X-ray diffractometer indicate that the biomolecular complex crystallizes in a monoclinic system, with lattice parameters a=7.86 Å, b=18.93 Å, and c=7.70 Å, yielding a



| Mode | Raman | FTIR Expt. | Scaled | Vibrational Assignments |
|------|-------|------------|------------|---|
| | Expt. | | Wavenumber | |
| 21 | | | 1821 | υ($C^{35} - H^{38}$)10, β($H^{37} - C^{35} - H^{36}$)14, |
| | | | | $\beta(H^{54} - O^{12} - C^5)14$, $\tau(H^{37} - C^{35} - N^{34} -$ |
| | | | | C^{25})46, $\tau(H^{54}-O^{12}-C^5-C^4)$ 46, $\tau(C^{31}=$ |
| | | | | $C^{30} - C^{29} - H^{54})46$, $\tau(C^4 - C^5 - N^6 -$ |
| | | | | C^{1})46, τ (C^{28} – C^{29} – H^{54} – O^{12})46 |
| 22 | 1687 | | 1666 | $υ(C^{44}-H^{49})33$, $β(H^{49}-C^{44}-C^{48})22$ |
| 23 | 1655 | 1639 | 1655 | $\upsilon(C^{25} = O^{39})31$, $\upsilon(C^{44} - H^{49})18$, $\tau(H^{20} -$ |
| | | | | $N^{19} - C^{16} - C^{14}$)19, $\tau(H^{21} - N^{19} - C^{16} -$ |
| | | | | C ¹⁴)13 |
| 24 | 1599 | | 1595 | $\upsilon(C^{25} = O^{39})88$, $\upsilon(N^{19} - H^{21})21$, $\upsilon(C^{14} - H^{21})$ |
| | | | | H^{22})17, $\beta(H^{22}-C^{14}-C^{16})24$ |
| 25 | 1521 | 1523 | 1539 | $υ(C^{42}-H^{45})15$, $β(H^{22}-C^{14}-C^{16})14$ |
| 26 | 1457 | 1442 | 1461 | $\beta(H^{50}-C^{46}-C^{48})15$ |
| 27 | 1398 | 1340 | 1348 | $\upsilon(C^{42}-H^{45})18$, $\tau(H^{45}-C^{42}-C^{44}-$ |
| | | | | C ⁴⁸)32 |
| 28 | 1262 | 1283 | 1230 | $\upsilon(C^{42}-H^{45})19$, $\tau(H^{45}-C^{42}-C^{44}-$ |
| | | | | C ⁴⁸)27 |
| 29 | 1240 | 1260 | 1199 | $\beta(H^{37}-C^{35}-H^{36})$ 12, $\beta(H^{54}-C^{12}-C^{12})$ |
| | 1100 | 1000 | 11== | C ⁵)12 |
| 30 | 1169 | 1200 | 1157 | $\tau(H^{27} - C^{23} - N^{33} = C^{24})18$ |
| 31 | 1130 | 1141 | 1118 | $\beta(H^{45}-C^{42}-C^{44})31$ |
| 32 | 1083 | 1054 | 1060 | $\upsilon(C^5 - C^6)10$, $\upsilon(C^{26} - C^{28})10$, $\beta(O^{12} -$ |
| | | | | $C^5 - C^6$)16, $\beta(N^{34} - C^{26} - C^{28})$ 16 |
| 33 | 1027 | | 1037 | $\beta(H^{45}-C^{42}-C^{44})23$ |
| 34 | | 1017 | 1019 | $\upsilon(C^5 - C^4)41, \gamma(O^{12} - C^4 - C^6 - C^5)14$ |
| 35 | | 917 | 910 | $\beta(C^2-C^1-C^6)13$ |
| 36 | | | 842 | $\tau(C^2-C^1-C^6-C^5)10$, $\tau(C^{30}-C^{29}-H^{54}-$ |
| | | | | O^{12})10, $\tau(N^{19}-C^{16}-C^{14}-C^3)$ 12 |
| 37 | | | 832 | $\upsilon(C^1-C^6)18$, $\tau(C^2-C^1-C^6-C^5)10$, |
| | | | | $\tau(C^{30}-C^{29}-H^{54}-O^{12})10$ |
| 38 | | 814 | 808 | υ(N ¹⁹ – C ¹⁶)14 |
| 39 | 792 | | 791 | $υ(C^{28} - H^{52})14$, $υ(C^{29} - H^{54})14$, $υ(C^{31} -$ |
| | | | | H ⁵⁵)10 |

Table 7 (Part 2): ν – stretching; τ – torsion; β – in-plane bending; γ – out-of-plane bending; Theoretical and experimental wavenumbers (cm⁻¹) and potential energy distribution for vibrational modes of Dopamine–Diazepam biomolecular complex to understand the type of vibrations for identifying the compositions.

unit cell volume of 111.79 ų. The angles are specified as $\alpha=90^\circ$, $\beta=103.55^\circ$, and $\gamma=90^\circ$ (Reference code: 00-031-1666). The PXRD pattern reveals reflections at 2θ values of 12°, 15°, 18°, 20°, 22°, 26°, 30°, 32°, 34°, 40°, 44°, 46°, 48°, 52°, 56°, 59°, 62°, 65°, 67°, 76°, 81°, and 89°, corresponding to interplanar distances (d) of 7.05 Å, 5.86 Å, 4.89 Å, 4.40 Å, 4.02 Å, 3.40 Å, 2.92 Å, 2.78 Å, 2.61 Å, 2.24 Å, 2.03 Å, 1.96 Å, 1.87 Å, 1.72 Å, 1.63 Å, 1.56 Å, 1.48 Å, 1.43 Å, 1.40 Å, 1.25 Å, 1.18 Å, and 1.10 Å, respectively. The average crystallite size of the synthesized biomolecular complex was calculated using Scherrer's formula [117]

$$D = \frac{\kappa \lambda}{\beta \cos \theta}.\tag{6}$$



| Mode | Raman Expt. | FTIR Expt. | Scaled Wavenumber | Vibrational Assignments |
|------|----------------|------------|----------------------|---|
| 40 | 753 | 741 | 742 | υ(C ³⁰ – Cl ⁴⁰)50 |
| 41 | | 704 | 707 | $\tau(H^{53}-C^{23}-N^{33}=C^{24})16$ |
| 42 | 693 | | 694 | $\beta(C^{31}-C^{30}-C^{29})12$, $\beta(C^{1}-C^{6}-C^{5})12$ |
| 43 | 650 | | 668 | $\upsilon(C^{43}-C^{46})15$ |
| 44 | | 630 | 623 | $\beta(O^{10}-C^6-C^1)13$ |
| 45 | 592 | 599 | 594 | $\beta(C^{32}-C^{31}=C^{30})11, \beta(C^{42}-C^{41}-C^{24})11$ |
| 46 | 551 | 551 | 564 | $\beta(O^{10}-C^6-C^1)16$ |
| 47 | | 467 | 474 | υ(C ³¹ – H ⁵⁵)12 |
| 48 | 440 | | 445 | $\beta(C^{48}-C^{44}-C^{42})16$ |
| 49 | | | 413 | $\upsilon(C^{25} = O^{39})12, \upsilon(C^{23} - C^{27})13$ |
| 50 | 396 | | 396 | υ(C ⁴² – C ⁴⁴)17 |
| 51 | | | 372 | $\upsilon(C^{25} = O^{39})10$, $\upsilon(Cl^{40} - C^{30})20$ |
| 52 | 357 | | 354 | $\upsilon(C^{23}-C^{27})24$ |
| 53 | | | 342 | $v(C^{24} = N^{33})13$ |
| 54 | 267 | | 264 | $\upsilon(C^{24} = N^{33})13, \upsilon(C^{26} - N^{34})20$ |
| 55 | 208 | | 205 | $\upsilon(C^{24} = N^{33})14$, $\beta(H^{51} - C^{31} - C^{32})10$ |
| 56 | | | 170 | $\upsilon(C^{29}-C^{30})16, \tau(C^{24}-C^{32}-C^{31}=C^{30})19, \gamma(C^{140}-C^{29}-C^{31}=C^{30})15$ |
| 57 | | | 152 | $\upsilon(C^{30} = C^{31})35$, $\tau(C^{26} - C^{28} - C^{29} - C^{30})12$, $\tau(C^{32} - C^{31} = C^{30} - C^{29})12$ |

Table 7 (Part 3): ν – stretching; τ – torsion; β – in-plane bending; γ – out-of-plane bending; Theoretical and experimental wavenumbers (cm⁻¹) and potential energy distribution for vibrational modes of Dopamine–Diazepam biomolecular complex to understand the type of vibrations for identifying the compositions.

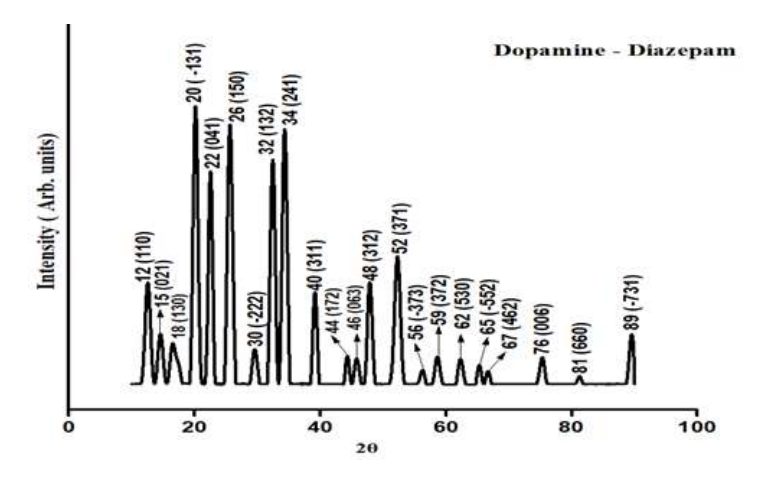


Figure 8: Powder X-ray diffraction pattern of Dopamine – Diazepam biomolecular complex.

Here, D represents the average grain size, $\kappa=0.891$ (Scherrer's constant), $\lambda=1.541874$ Å (wavelength of the X-ray), β is the FWHM (Full Width at Half Maximum), and θ is the diffraction angle. Using Scherrer's formula, the average value of D is calculated to be 10.90 nm. Table 8 provides the peak positions (2θ) , cor-



| Sl.no | 2θ (°) | d [Å] | β (FWHM) | Miller indices |
|-------|--------|-------|----------|----------------|
| 1 | 12 | 7.05 | 0.95 | 110 |
| 2 | 15 | 5.86 | 0.85 | 021 |
| 3 | 18 | 4.89 | 1.32 | 130 |
| 4 | 20 | 4.40 | 0.86 | -131 |
| 5 | 22 | 4.02 | 0.75 | 041 |
| 6 | 26 | 3.40 | 0.91 | 150 |
| 7 | 30 | 2.92 | 0.85 | -222 |
| 8 | 32 | 2.78 | 0.85 | 132 |
| 9 | 34 | 2.61 | 0.86 | 241 |
| 10 | 40 | 2.24 | 0.73 | 311 |
| 11 | 44 | 2.03 | 0.64 | 172 |
| 12 | 46 | 1.96 | 0.78 | 063 |
| 13 | 48 | 1.87 | 0.84 | 312 |
| 14 | 52 | 1.72 | 1.04 | 371 |
| 15 | 56 | 1.63 | 0.79 | -373 |
| 16 | 59 | 1.56 | 0.87 | 372 |
| 17 | 62 | 1.48 | 0.85 | 530 |
| 18 | 65 | 1.43 | 0.67 | -552 |
| 19 | 67 | 1.40 | 0.69 | 462 |
| 20 | 76 | 1.25 | 0.85 | 006 |
| 21 | 81 | 1.18 | 0.70 | 660 |
| 22 | 89 | 1.10 | 0.78 | -731 |

Table 8: Peak positions (2θ) along with corresponding interplanar distances (d) and F.W.H.M. (Full wave at half maximum), Miller indices of Dopamine – Diazepam biomolecular complex

responding interplanar distances (d), FWHM, and Miller indices. The powder X-ray diffraction pattern of the Dopamine–Diazepam biomolecular complex, including peak positions with Miller indices indicated in brackets, is shown in figure 8.

4 Analysis of Molecular Docking

Molecular docking is a widely used virtual screening technique designed to predict potential binding sites in ligand-receptor interactions, following the Lock and Key model [118, 119]. In this study, Autodock software was employed to evaluate the potential of the Dopamine–Diazepam biomolecular complex against the 7CKW and 7X2F D1 Dopamine receptor protein. The 7CKW and 7X2F protein, a Dopamine receptor, were obtained from the RCSB PDB database. Docking procedures adhered to established protocols. Initially, the downloaded protein file (in PDB format) contained water molecules, heteroatoms, and ligands, which were removed using BIOVIA Discovery Studio 2021. Hydrogen atoms and Gasteiger charges were then added using UCSF Chimera tools. The prepared protein was saved in PDB format and converted to PDBQT format, ensuring a stable and energetically optimized structure. Docking was carried out following standard protocols, generating 10 docking conformations. The conformation with the highest binding energy was selected and visualized using BIOVIA Discovery Studio 2021. Figure 9a shows the interactions between the protein 7CKW and the ligand Dopamine–Diazepam. Figure 9b highlights the 2D ligand–7CKW protein interaction while figure 9c depicts the 2D ligand–7X2F protein interaction with specific amino acid residues.

The 7CKW and 7X2F D1 Dopamine receptor proteins are G-protein coupled receptors crucial for a variety of daily functions, influencing movement, emotions, and the brain's reward system, which is expressed by the gene 5q31-q34 with positive allosteric modulator for endogenous Dopamine [120]. These receptors are primarily found in the central nervous system, particularly in the hippocampal dentate gyrus and subventricular zone. Additionally, dopamine receptors are expressed in peripheral tissues, with a notable presence in the kidney and blood vessels. Table 9 summarizes the best binding energies and corresponding hydrogen bond distances.



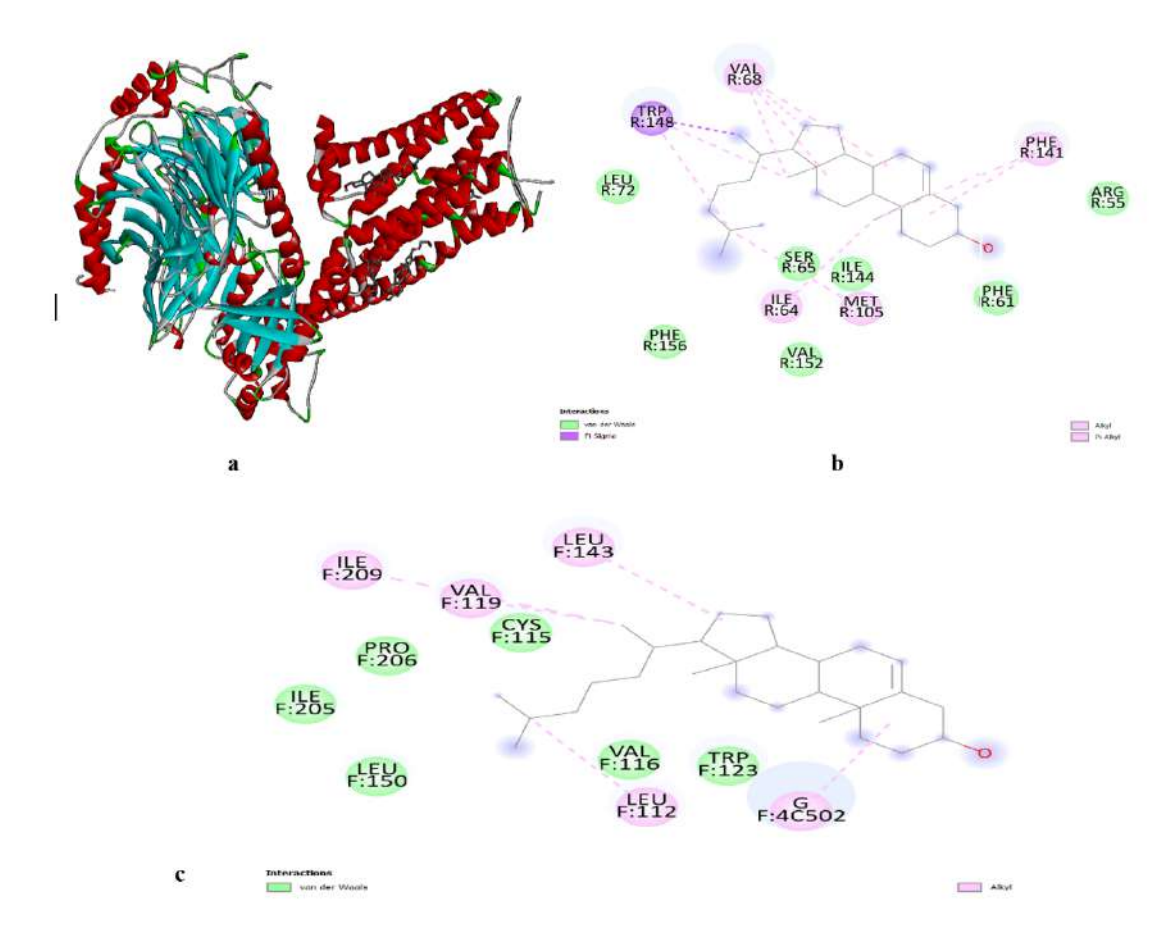


Figure 9: Dopamine – Diazepam biomolecular complex (a) Interaction with 7CKW (b) 2D representation with 7CKW (c) 2D representation with 7X2F.

The binding energy of the Dopamine–Diazepam complex with 7CKW is determined to be -8.37 kcal/mol while with 7X2F is -7.92 kcal/mol. It is found that 7CKW has better binding affinity than 7X2F with the chosen ligand (Dopamine–Diazepam), signifying more reactive and spontaneous interaction with superior antianxiety activity [121].

5 Conclusion

The Dopamine–Diazepam biomolecular complex exhibits a low HOMO-LUMO gap and a high electrophilicity index, indicating substantial chemical reactivity, strong electrophilic properties, and notable bioactivity. MEP mapping highlights active sites for electronegative regions near oxygen atoms with red color and electropositive regions near hydrogen atoms with blue color. NBO analysis confirms charge transfer within the complex, revealing a maximum stabilization energy of 251.96 kJ/mol. AIM analysis identifies intermolecular hydrogen bond formation at BCP 29 (H¹³–O¹²–H⁵⁴) with covalent nature, and at BCP 66 (H¹³–O¹²–Cl⁴⁰) with electrostatic characteristics, emphasizing the molecules' active interactions.

Additionally, RDG analysis identifies van der Waals and hydrogen bonding interactions through a color-coded isosurface, further elucidating the stability and interaction mechanisms of the biomolecular complex. Quantum parameters, such as hardness and chemical potential, indicate the complex's resistance to decomposition and higher polarizability, contributing to its stability. Lipinski's criteria classify the complex as having good oral bioavailability, with a toxicity rating of class IV. It was found that theoretical and experimental peaks have a good correlation. Molecular docking studies reveal strong binding affinities of selected proteins with the Dopamine–Diazepam com-



| Ligand | Receptor (PDB ID) | Binding Energy (kcal/mol) | Binding residue | Interactions | Bond Length |
|---------------------|----------------------|------------------------------|--------------------|--------------|-------------|
| Dopamine – Diazepam | 7CKW | -8.37 | R:VAL68 | Alkyl | 5.22 |
| | | | R:VAL68 | Alkyl | 5.09 |
| | | | R:VAL68 | Alkyl | 3.97 |
| | | | R:VAL68 | Alkyl | 3.70 |
| | | | R:TRP148 | Pi – alkyl | 3.94 |
| | | | R:TRP148 | Pi – Alkyl | 5.22 |
| | 2 | | R:TRP148 | Pi – sigma | 4.54 |
| | | | R:PHE141 | Pi – alkyl | 5.44 |
| | 0.1 | | R:PHE141 | Pi – alkyl | 4.93 |
| | | | R:ILE64 | Alkyl | 4.54 |
| | | | R:MET105 | Alkyl | 4.67 |
| Dopamine – Diazepam | 7X2F | - 7.92 | F:LEU143 | Alkyl | 5.48 |
| | | | F:ILE209 | Alkyl | 4.50 |
| | | | F:VAL119 | Alkyl | 4.38 |
| | | | F:LEU112 | Alkyl | 4.50 |
| | | | F:G4C502 | Alkyl | 3.91 |

Table 9: Amino acid residues, types of binding, bond distances, and binding energy analysis of Dopamine – Diazepam biomolecular complex with 7CKW and 7X2F receptor.

plex, with excellent binding energies. X-ray diffraction confirms co-crystal formation.

Acknowledgement

We express our gratitude to the University Grants Commission (UGC) funded Central Facility for providing XRD and FTIR instrumentation at the Department of Physics, Manipur University, Manipur, India. We also appreciate the support from the Science and Engineering Research Board (SERB)-Power Grant project, Department of Physics, Manipur University, for providing instrumentation facilities to record Raman spectra. Our sincere thanks go to the UGC SAP, DRS-II, Department of Physics, Manipur University, for offering computational facilities, particularly Gaussian 16. One of the authors, Lamthaka Willingson, is also grateful to National Fellowship for Higher Education of ST Students (NFST) (Award No. 202223-NFST-MAN-01081) for financial support during this research.



A Supplementary tables

| e Å] DFT/B31YP/ 6-311++ g(d,p) m DFT/B31YP/ 6-311++ g(d,p) 1. N¹¹¹ − H²¹¹ 1.016 C²² − H²²¹ 1.084 2. N¹² − C¹¹ 1.016 C²² − H²²² 1.083 3. N¹² − C¹¹ 1.468 C²² − H²²³ 1.084 4. C¹¹ − H³³ 1.094 C²² − H²³ 1.084 5. C¹² − H³³ 1.101 C²¹ − H²⁵ 1.082 6. C³⁴ − C¹² 1.537 C¹³ − C²¹ 1.403 7. C¹⁴ − H³⁵ 1.094 C²¹ − C²¹ 1.403 8. C¹⁴ − C³¹ 1.512 C²² − C²² 1.344 8. C¹⁴ − C³ 1.512 C²² − C²² 1.392 10. C³ − C² 1.397 C²² − C²² 1.392 11. C² − H³ 1.085 C²° − C¹³ 1.401 12. C² − C¹ 1.395 C¹³ − C² 1.493 13. C¹ − H² 1.084 C² − C¹³ 1.401 14. C¹ − C² 1.389 C¹° − C² 1.392 17. C² − C² 1.401 <td< th=""><th>SI. No.</th><th>Bond in Dopamin</th><th>Bond length of Dopamine [</th><th>Bond in Diazepa</th><th>Bond length of Diazepam [Å]</th></td<> | SI. No. | Bond in Dopamin | Bond length of Dopamine [| Bond in Diazepa | Bond length of Diazepam [Å] |
|---|------------|-----------------------------------|------------------------------|-----------------------------------|---------------------------------|
| 1. N ¹⁹ − H ²⁰ 1.016 C ²² − H ²⁷ 1.084 2. N ¹⁹ − H ²¹ 1.016 C ²⁰ − H ²² 1.083 3. N ¹⁹ − C ¹⁶ 1.468 C ²⁶ − H ²⁹ 1.084 4. C ¹⁶ − H ¹⁸ 1.094 C ²⁴ − H ²⁸ 1.084 5. C ¹⁶ − H ¹⁷ 1.101 C ²¹ − H ²⁵ 1.082 6. C ¹⁴ − C ¹⁶ 1.537 C ¹⁹ − C ²¹ 1.403 7. C ¹⁴ − H ¹⁵ 1.094 C ²¹ − C ²⁴ 1.34 8. C ¹⁴ − C ³ 1.512 C ²⁶ − C ²² 1.392 10. C ³ − C ² 1.397 C ²² − C ³ 1.393 11. C ² − H ⁸ 1.085 C ²⁰ − C ³ 1.401 12. C ² − C ¹ 1.395 C ³ − C ² 1.493 13. C ¹ − H ⁷ 1.084 C ²⁰ − C ²⁰ 1.491 14. C ¹ − C ⁶ 1.389 C ¹⁰ − C ⁹ 1.404 15. C ⁶ − O ¹⁰ 1.365 C ⁹ − C ⁸ 1.385 16. O ¹⁰ − H ¹¹ 0.966 C ⁸ − C ⁷ 1.392 17. C ⁶ − C ⁵ 1.401 C ⁷ − C ⁶ 1.387 18. C ⁵ − O ¹² 1.379 C ⁶ − C ⁶ 1.404 20. C ⁶ − C ⁷ 1.388 C ⁹ − C ⁶ 1.404 21. C ⁶ − C ⁵ 1.401 C ⁷ − C ⁶ 1.404 22. C ⁶ − C ⁷ 1.388 C ⁹ − C ⁸ 1.387 23. C ⁶ − C ⁴ 1.404 24. C ⁶ − C ⁵ 1.401 C ⁷ − C ⁶ 1.404 25. C ⁶ − C ⁴ 1.388 C ⁶ − C ¹⁸ 1.757 22. C ⁴ − C ³ 1.401 C ⁷ − C ⁶ − C ¹⁸ 1.757 22. C ⁴ − C ³ 1.392 24. C ⁶ − C ¹⁹ 1.416 25. N ¹² − C ³ 1.392 26. C ⁶ − N ¹¹ 1.525 27. C ¹ − N ¹¹ 1.454 | | e | | m | |
| 1. $N^{19} - H^{20}$ 1.016 $C^{22} - H^{27}$ 1.084 2. $N^{19} - H^{21}$ 1.016 $C^{20} - H^{22}$ 1.083 3. $N^{19} - C^{16}$ 1.468 $C^{26} - H^{29}$ 1.084 4. $C^{16} - H^{18}$ 1.094 $C^{24} - H^{28}$ 1.084 5. $C^{16} - H^{17}$ 1.101 $C^{21} - H^{25}$ 1.082 6. $C^{14} - C^{16}$ 1.537 $C^{19} - C^{21}$ 1.403 7. $C^{14} - H^{15}$ 1.094 $C^{21} - C^{24}$ 1.34 8. $C^{14} - H^{22}$ 1.096 $C^{24} - C^{26}$ 1.34 9. $C^{14} - C^{3}$ 1.512 $C^{26} - C^{22}$ 1.392 10. $C^{3} - C^{2}$ 1.397 $C^{22} - C^{20}$ 1.393 11. $C^{2} - H^{8}$ 1.085 $C^{20} - C^{29}$ 1.401 12. $C^{2} - C^{1}$ 1.395 $C^{19} - C^{2}$ 1.493 13. $C^{1} - H^{7}$ 1.084 $C^{2} - C^{10}$ 1.491 14. $C^{1} - C^{6}$ 1.389 $C^{10} - C^{9}$ 1.404 | | | | | 6-311++ g(d,p) |
| 2. N¹9 − H²¹ 1.016 C²0 − H²² 1.083 3. N¹9 − C³6 1.468 C²6 − H²³ 1.084 4. C¹6 − H³8 1.094 C²⁴ − H²8 1.084 5. C¹6 − H³² 1.101 C²³ − H²³ 1.082 6. C¹⁴ − C¹6 1.537 C¹³ − C²¹ 1.403 7. C¹⁴ − H³⁵ 1.094 C²² − C²⁴ 1.34 8. C¹⁴ − H²² 1.096 C²⁴ − C²6 1.34 9. C¹⁴ − C³ 1.512 C²² − C²² 1.392 10. C³ − C² 1.397 C²² − C²⁰ 1.393 11. C² − H³ 1.085 C²⁰ − C³³ 1.401 12. C² − C¹ 1.395 C¹³ − C²³ 1.493 13. C¹ − H² 1.084 C² − C¹³ 1.491 14. C¹ − C² 1.389 C¹³ − C²³ 1.404 15. C² − O¹³ 1.365 C² − C² 1.385 16. O¹³ − H¹¹ 0.966 C² − C² 1.387 17. C² − C² 1.401 C² − C² 1.413 | | | 6-311++ g(d,p) | | |
| $\begin{array}{c ccccccccccccccccccccccccccccccccccc$ | 1. | N ¹⁹ - H ²⁰ | 1.016 | C ²² – H ²⁷ | 1.084 |
| $ \begin{array}{c ccccccccccccccccccccccccccccccccccc$ | 2. | N ¹⁹ - H ²¹ | 1.016 | C ²⁰ – H ²² | 1.083 |
| $\begin{array}{cccccccccccccccccccccccccccccccccccc$ | 3. | N ¹⁹ - C ¹⁶ | 1.468 | C ²⁶ – H ²⁹ | 1.084 |
| $\begin{array}{cccccccccccccccccccccccccccccccccccc$ | 4. | C ¹⁶ - H ¹⁸ | 1.094 | C ²⁴ - H ²⁸ | 1.084 |
| $\begin{array}{cccccccccccccccccccccccccccccccccccc$ | 5. | C ¹⁶ - H ¹⁷ | 1.101 | C ²¹ – H ²⁵ | 1.082 |
| $\begin{array}{cccccccccccccccccccccccccccccccccccc$ | 6. | C14 - C16 | 1.537 | C19 - C21 | 1.403 |
| $\begin{array}{cccccccccccccccccccccccccccccccccccc$ | 7. | C14 - H15 | 1.094 | C ²¹ - C ²⁴ | 1.34 |
| $\begin{array}{c ccccccccccccccccccccccccccccccccccc$ | 8. | C14 - H22 | 1.096 | C ²⁴ – C ²⁶ | 1.34 |
| 11. $C^2 - H^8$ 1.085 $C^{20} - C^{19}$ 1.401 12. $C^2 - C^1$ 1.395 $C^{19} - C^2$ 1.493 13. $C^1 - H^7$ 1.084 $C^2 - C^{10}$ 1.491 14. $C^1 - C^6$ 1.389 $C^{10} - C^9$ 1.404 15. $C^6 - O^{10}$ 1.365 $C^9 = C^8$ 1.385 16. $O^{10} - H^{11}$ 0.966 $C^8 - C^7$ 1.392 17. $C^6 - C^3$ 1.401 $C^7 - C^6$ 1.387 18. $C^5 - O^{12}$ 1.379 $C^6 - C^4$ 1.404 19. $O^{12} - H^{13}$ 0.962 $C^4 - C^{10}$ 1.413 20. $C^5 - C^4$ 1.388 $C^9 - H^{33}$ 1.082 21. $C^4 - H^9$ 1.087 $C^8 - C^{18}$ 1.757 22. $C^4 - C^3$ 1.401 $C^7 - H^{32}$ 1.082 23. $C^6 - H^{30}$ 1.082 24. $C^8 - C^1$ 1.416 25. $N^{12} - C^3$ 1.392 26. $C^3 - C^1$ 1.525 27. | 9. | C14 - C3 | 1.512 | C ²⁶ – C ²² | 1.392 |
| $\begin{array}{cccccccccccccccccccccccccccccccccccc$ | 10. | C3 - C2 | 1.397 | C22 - C20 | 1.393 |
| $\begin{array}{c ccccccccccccccccccccccccccccccccccc$ | 11. | C ² - H ⁸ | 1.085 | | 1.401 |
| 14. $C^1 - C^6$ 1.389 $C^{10} - C^9$ 1.404 15. $C^6 - O^{10}$ 1.365 $C^9 - C^8$ 1.385 16. $O^{10} - H^{11}$ 0.966 $C^8 - C^7$ 1.392 17. $C^6 - C^5$ 1.401 $C^7 - C^6$ 1.387 18. $C^5 - O^{12}$ 1.379 $C^6 - C^4$ 1.404 19. $O^{12} - H^{13}$ 0.962 $C^4 - C^{10}$ 1.413 20. $C^5 - C^4$ 1.388 $C^9 - H^{33}$ 1.082 21. $C^4 - H^9$ 1.087 $C^8 - Cl^{18}$ 1.757 22. $C^4 - C^3$ 1.401 $C^7 - H^{32}$ 1.082 23. $C^6 - H^{30}$ 1.082 24. $C^4 - N^{12}$ 1.416 25. $N^{12} - C^3$ 1.392 26. $C^3 - C^1$ 1.525 27. $C^1 - N^{11}$ 1.454 | 12. | C2 - C1 | 1.395 | | 1.493 |
| $\begin{array}{c ccccccccccccccccccccccccccccccccccc$ | 13. | C1 - H7 | 1.084 | | 1.491 |
| 16. $O^{10} - H^{11}$ $O.966$ $C^8 - C^7$ 1.392 17. $C^6 - C^5$ 1.401 $C^7 - C^6$ 1.387 18. $C^5 - O^{12}$ 1.379 $C^6 - C^4$ 1.404 19. $O^{12} - H^{13}$ 0.962 $C^4 - C^{10}$ 1.413 20. $C^5 - C^4$ 1.388 $C^9 - H^{33}$ 1.082 21. $C^4 - H^9$ 1.087 $C^8 - Cl^{18}$ 1.757 22. $C^4 - C^3$ 1.401 $C^7 - H^{32}$ 1.082 23. $C^6 - H^{30}$ 1.082 24. $C^4 - N^{12}$ 1.416 25. $N^{12} - C^3$ 1.392 26. $C^3 - C^1$ 1.525 27. $C^1 - N^{11}$ 1.454 | 14. | C1 - C6 | 1.389 | C10 - C9 | 1.404 |
| $ \begin{array}{cccccccccccccccccccccccccccccccccccc$ | 15. | C6 - O10 | 1.365 | C9 = C8 | 1.385 |
| $ \begin{array}{cccccccccccccccccccccccccccccccccccc$ | 16. | O ¹⁰ - H ¹¹ | 0.966 | C8 - C7 | 1.392 |
| $\begin{array}{cccccccccccccccccccccccccccccccccccc$ | 17. | C6-C5 | 1.401 | C7 - C6 | 1.387 |
| $ \begin{array}{cccccccccccccccccccccccccccccccccccc$ | 18. | C5 - O12 | 1.379 | C6 - C4 | 1.404 |
| $ \begin{array}{cccccccccccccccccccccccccccccccccccc$ | 19. | O ¹² - H ¹³ | 0.962 | C4-C10 | 1.413 |
| $ \begin{array}{c ccccccccccccccccccccccccccccccccccc$ | 20. | C5 - C4 | 1.388 | C9 - H33 | 1.082 |
| $ \begin{array}{c cccc} 23. & & & & & & & & & & \\ 24. & & & & & & & & & \\ 25. & & & & & & & & \\ 26. & & & & & & & \\ 27. & & & & & & & \\ \end{array} $ | 21. | C4 - H9 | 1.087 | C8 - CI18 | 1.757 |
| $ \begin{array}{c cccc} 24. & & & & & & & & & & \\ 25. & & & & & & & & \\ 25. & & & & & & & \\ 26. & & & & & & & \\ 27. & & & & & & & \\ \end{array} \qquad \begin{array}{c cccc} C^4-N^{12} & 1.416 & & & \\ 1.392 & & & & \\ 27. & & & & & \\ 27. & & & & & \\ \end{array} $ | 22. | C4 - C3 | 1.401 | C7 - H32 | 1.082 |
| 25. N ¹² - C ³ 1.392 26. C ³ - C ¹ 1.525 27. C ¹ - N ¹¹ 1.454 | 23. | | | C ₆ - H ₃₀ | 1.082 |
| 26. C³-C¹ 1.525 27. C¹-N¹¹ 1.454 | 24. | | | C4 - N12 | 1.416 |
| 27. C¹-N¹¹ 1.454 | 25. | | | N ¹² - C ³ | 1.392 |
| | 26. | | | C3 - C1 | 1.525 |
| $N^{11} = C^2 - 1.282$ | 27. | | | C1 - N11 | 1.454 |
| 20. 1.202 | 28. | | | N ¹¹ = C ² | 1.282 |

| SI. No. | Bond in Dopamine | Bond length of Dopamine [Å] DFT/B3LYP/ 6-311++ g(d,p) | Bond in Diazepam | Bond length of Diazepam [Å] DFT/B3LYP/ 6-311++ g(d,p) |
|---------|---------------------|--|-----------------------------------|---|
| 29. | | | C1 - H5 | 1.088 |
| 30. | | | C1- H31 | 1.1 |
| 31. | | | C3 = O17 | 1.214 |
| 32. | | | C13 - H14 | 1.089 |
| 33. | | | C13 - H15 | 1.095 |
| 34. | | | C13 - H16 | 1.088 |
| 35. | | | N ¹² - C ¹³ | 1.468 |

Table S-1: Bond lengths of Optimized structure of Dopamine, and Diazepam monomers.



| Donor (i) | Acceptor (j) | E (2) | E(j) - E(i) | F _{i,j} |
|--|---------------------------------------|----------|-------------|------------------|
| | | (kJ/mol) | (a.u) | (a.u) |
| Within Dopamine | | | | |
| $\sigma(C^1-C^2)$ | $\sigma^*(C^2 - C^3)$ | 3.36 | 1.28 | 0.059 |
| $\sigma(C^1-C^2)$ | $\sigma^*(C^3 - O^{14})$ | 3.67 | 1.13 | 0.058 |
| $\sigma(C^1-C^2)$ | $\sigma^*(C^6 - O^{10})$ | 4.11 | 1.05 | 0.059 |
| $\pi(C^1 - C^2)$ | $\pi^*(C^3 - C^4)$ | 20.2 | 0.29 | 0.069 |
| $\pi(C^1-C^2)$ | $\pi^*(C^5 - C^6)$ | 20.49 | 0.27 | 0.069 |
| $\sigma(C^1-C^6)$ | $\sigma^*(C^5 - C^6)$ | 3.77 | 1.25 | 0.061 |
| $\sigma(C^1-C^6)$ | $\sigma^*(C^5 - O^{12})$ | 3.37 | 1.03 | 0.053 |
| $\sigma(C^1 - H^7)$ | $\sigma^*(C^5 - C^3)$ | 3.63 | 1.1 | 0.057 |
| $\sigma(C^1 - H^7)$ | $\sigma^*(C^5 - C^3)$ | 3.76 | 1.06 | 0.057 |
| $\sigma(C^2-C^3)$ | $\sigma^*(C^1 - C^2)$ | 3.1 | 1.28 | 0.056 |
| $\sigma(C^2-C^3)$ | $\sigma^*(C^3 - C^4)$ | 3.2 | 1.27 | 0.057 |
| $\sigma(C^2 - H^8)$ | $\sigma^*(C^3 - C^4)$ | 4.68 | 1.09 | 0.064 |
| $\sigma(C^2 - H^8)$ | $\sigma^*(C^1 - C^6)$ | 3.33 | 1.07 | 0.053 |
| $\sigma(C^3-C^4)$ | $\sigma^*(C^2 - C^3)$ | 3.16 | 1.28 | 0.057 |
| $\sigma(C^3-C^4)$ | $\sigma^*(C^4 - C^5)$ | 3.26 | 1.26 | 0.057 |
| $\sigma(C^3 - C^4)$ | $\sigma^*(C^5 - O^{12})$ | 4.52 | 1.01 | 0.061 |
| $\pi(C^3 - C^4)$ | $\pi^*(C^1 - C^2)$ | 19.35 | 0.28 | 0.067 |
| $\pi(C^3 - C^4)$ | $\pi^*(C^5 - C^6)$ | 22.32 | 0.27 | 0.071 |
| $\sigma^*(C^3 - C^{14})$ | $\sigma^*(C^3 - C^4)$ | 10.42 | 1.2 | 0.044 |
| $\sigma^*(C^3 - C^{14})$ | $\sigma^*(C^4 - C^5)$ | 4.76 | 1.18 | 0.046 |
| $\sigma(C^4-C^5)$ | $\sigma^*(C^3 - C^4)$ | 3.56 | 1.3 | 0.061 |
| $\sigma(C^4-C^5)$ | $\sigma^*(C^3 - C^{14})$ | 3.21 | 1.15 | 0.054 |
| $\sigma(C^4-C^5)$ | $\sigma^*(C^5 - C^6)$ | 4.27 | 1.26 | 0.066 |
| $\sigma(C^4-C^5)$ | σ*(C ⁶ – O ¹⁰) | 3.44 | 1.07 | 0.054 |
| $\sigma(C^4 - H^9)$ | $\sigma^*(C^2 - C^3)$ | 4.38 | 1.1 | 0.062 |
| $\sigma(C^4 - H^9)$ | $\sigma^*(C^5 - C^6)$ | 3.96 | 1.06 | 0.058 |
| $\sigma(C^5-C^6)$ | $\sigma^*(C^1 - C^6)$ | 3.97 | 1.28 | 0.064 |
| $\sigma(C^5-C^6)$ | $\sigma^*(C^4 - C^5)$ | 4.04 | 1.28 | 0.064 |
| $\pi(C^5 - C^6)$ | $\pi^*(C^1 - C^2)$ | 19.66 | 0.3 | 0.069 |
| $\pi(C^5 - C^6)$ | $\pi^*(C^3 - C^4)$ | 19.82 | 0.3 | 0.069 |
| σ*(O ¹⁰ – H ¹¹) | $\sigma^*(C^1 - C^6)$ | 4.43 | 1.31 | 0.068 |
| σ*(O ¹² – H ¹³) | $\sigma^*(C^5 - C^6)$ | 3.1 | 1.3 | 0.057 |
| $\sigma(C^{14}-C^{15})$ | $\sigma^*(C^2 - C^3)$ | 3.76 | 1.07 | 0.057 |
| $\sigma(C^{14} - H^{22})$ | $\sigma^*(C^3 - C^4)$ | 3.82 | 1.06 | 0.057 |
| $\sigma(C^{16} - H^{18})$ | $\sigma^*(N^{19} - H^{21})$ | 3.14 | 0.93 | 0.048 |
| n ₁ (O ¹⁰) | $\sigma^*(C^5 - C^6)$ | 5.52 | 1.15 | 0.071 |
| n ₂ (O ¹⁰) | $\pi^*(C^5 - C^6)$ | 26.04 | 0.35 | 0.092 |

Table S-2 (part 1): Second-order perturbation theory analysis of Fock Matrix in NBO Basis of Dopamine - Diazepam biomolecular complex to understand the intra and intermolecular charge transfer.



| Donor (i) | Acceptor (j) | E (2) | E(j) - E(i) | F _{i,j} |
|---------------------------------------|--|----------|-------------|------------------|
| | | (kJ/mol) | (a.u) | (a.u) |
| n ₁ (O ¹²) | $\sigma^*(C^4 - C^5)$ | 5.93 | 1.19 | 0.075 |
| n ₂ (O ¹²) | π*(C ⁵ – C ⁶) | 20.34 | 0.36 | 0.084 |
| n ₁ (N ¹⁹) | $\sigma^*(C^{16} - H^{17})$ | 7.33 | 0.71 | 0.064 |
| $\pi^*(C^5 - C^6)$ | $\pi^*(C^1 - C^2)$ | 251.96 | 0.01 | 0.082 |
| $\pi^*(C^5 - C^6)$ | $\pi^*(C^3 - C^4)$ | 196.83 | 0.02 | 0.082 |
| From Dopamine to | | | | |
| Diazepam | | | | |
| $\pi(C^3-C^4)$ | $\sigma^*(C^{46}-C^{48})$ | 0.08 | 3.78 | 0.017 |
| n ₁ (O ¹⁰) | $\sigma^*(C^{46} - H^{50})$ | 0.05 | 4.68 | 0.014 |
| n ₁ (O ¹²) | $\sigma^*(C^{29}-C^{54})$ | 0.74 | 1.06 | 0.025 |
| $n_2(O^{12})$ | σ*(C ²⁹ – C ⁵⁴) | 0.71 | 0.78 | 0.022 |
| From Diazepam to | | | | |
| Dopamine | | | | |
| n ₂ (Cl ⁴⁰) | σ*(O ¹⁰ – H ¹¹) | 0.52 | 0.75 | 0.018 |
| n ₃ (Cl ⁴⁰) | $\sigma^*(O^{10} - H^{11})$ | 0.29 | 0.75 | 0.013 |
| Diazepam | | | | |
| $\sigma(C^{23}-C^{25})$ | $\sigma^*(N^{34}-C^{35})$ | 4.14 | 0.96 | 0.057 |
| $\sigma(C^{23} - H^{27})$ | $\sigma^*(C^{24} = N^{33})$ | 3.3 | 1.12 | 0.054 |
| $\sigma(C^{23} - H^{27})$ | $\sigma^*(C^{25} - N^{34})$ | 4.12 | 0.93 | 0.056 |
| $\sigma(C^{23} - N^{33})$ | $\sigma^*(C^{24}-C^{41})$ | 5.23 | 1.17 | 0.07 |
| $\sigma(C^{24}-C^{32})$ | $\sigma^*(C^{26}-C^{28})$ | 3.61 | 1.2 | 0.059 |
| $\sigma(C^{24}=N^{33})$ | $\sigma^*(C^{23}-C^{25})$ | 3.59 | 0.7 | 0.045 |
| $\sigma(C^{24} = N^{33})$ | $\pi^*(C^{41}-C^{42})$ | 6.07 | 0.36 | 0.045 |
| $\sigma(C^{24}-C^{41})$ | $\sigma^*(C^{23} - N^{33})$ | 4.77 | 1.02 | 0.063 |
| $\sigma(C^{26}-C^{28})$ | $\sigma^*(C^{24}-C^{32})$ | 3.15 | 1.14 | 0.045 |
| $\sigma(C^{26}-C^{28})$ | $\sigma^*(C^{26}-C^{32})$ | 5.08 | 1.26 | 0.072 |
| $\pi(C^{26}-C^{28})$ | $\pi^*(C^{29}-C^{30})$ | 23.06 | 0.28 | 0.072 |
| $\pi(C^{26}-C^{28})$ | $\pi^*(C^{31}-C^{32})$ | 19.04 | 0.32 | 0.069 |
| $\sigma(C^{26}-C^{32})$ | $\sigma^*(C^{26}-C^{28})$ | 4.01 | 1.25 | 0.064 |
| $\sigma(C^{28}-C^{29})$ | $\sigma^*(C^{26}-C^{28})$ | 3.22 | 1.26 | 0.057 |
| $\sigma(C^{28}-C^{29})$ | $\sigma^*(C^{30} - CI^{40})$ | 5.29 | 0.85 | 0.06 |
| σ(C ²⁸ – H ⁵²) | $\sigma^*(C^{26}-C^{32})$ | 4.39 | 1.08 | 0.061 |
| σ(C ²⁸ – H ⁵²) | $\sigma^*(C^{29}-C^{30})$ | 3.42 | 1.08 | 0.054 |
| $\sigma(C^{29}-C^{30})$ | $\sigma^*(C^{30}-C^{31})$ | 3.79 | 1.3 | 0.063 |
| $\sigma(C^{29}-C^{30})$ | π*(C ²⁶ – C ²⁸) | 18.29 | 0.29 | 0.066 |
| $\sigma(C^{29}-C^{30})$ | $\pi^*(C^{31}-C^{32})$ | 20.42 | 0.33 | 0.073 |
| $\sigma(C^{29} - H^{54})$ | σ*(C ²⁶ – C ²⁸) | 3.9 | 1.07 | 0.058 |
| $\sigma(C^{29} - H^{54})$ | $\sigma^*(C^{30}-C^{31})$ | 4.26 | 1.1 | 0.061 |
| $\sigma(C^{30}-C^{31})$ | $\sigma^*(C^{31}-C^{32})$ | 4.12 | 1.32 | 0.066 |
| $\sigma(C^{30}-C^{31})$ | σ*(C ⁴⁶ – C ⁴⁸) | 28.14 | 4.28 | 0.31 |
| $\sigma(C^{30}-C^{31})$ | σ*(C ⁴⁶ – H ⁵⁰) | 17.28 | 4.82 | 0.258 |
| $\sigma(C^{31}-C^{32})$ | $\sigma^*(C^{26}-N^{34})$ | 5.36 | 1.1 | 0.069 |

Table S-2 (part 2): Second-order perturbation theory analysis of Fock Matrix in NBO Basis of Dopamine - Diazepam biomolecular complex to understand the intra and intermolecular charge transfer.



| Donor (i) | Acceptor (j) | E (²) | E(j) - E(i) | F _{i,j} |
|---------------------------------------|--|----------|-------------|------------------|
| | | (kJ/mol) | (a.u) | (a.u) |
| $\sigma(C^{31}-C^{32})$ | $\sigma^*(C^{26}-N^{34})$ | 5.36 | 1.1 | 0.069 |
| $\sigma(C^{31}-C^{32})$ | $\sigma^*(C^{30} - CI^{40})$ | 5.3 | 0.83 | 0.06 |
| $\sigma(C^{31}-C^{32})$ | $\sigma^*(C^{46}-C^{48})$ | 5.1 | 4.24 | 0.132 |
| $\sigma(C^{31}-C^{32})$ | σ*(C ⁴⁶ – H ⁵⁰) | 32.57 | 4.78 | 0.355 |
| $\sigma(C^{31}-C^{32})$ | $\sigma^*(C^{46} - H^{51})$ | 4.17 | 2.93 | 0.1 |
| $\pi(C^{31}-C^{32})$ | $\pi^*(C^{24} = N^{33})$ | 11.94 | 0.28 | 0.054 |
| $\pi(C^{31}-C^{32})$ | $\pi^*(C^{26}-C^{28})$ | 23.93 | 0.26 | 0.071 |
| $\pi(C^{31}-C^{32})$ | $\pi^*(C^{29}-C^{30})$ | 20.07 | 0.26 | 0.071 |
| $\sigma(C^{31} - H^{55})$ | $\sigma^*(C^{26}-C^{32})$ | 4.09 | 1.07 | 0.059 |
| $\sigma(C^{31} - H^{55})$ | $\sigma^*(C^{29}-C^{30})$ | 4.26 | 1.07 | 0.06 |
| $\sigma(C^{31} - H^{55})$ | $\sigma^*(C^{46}-C^{48})$ | 35.03 | 4.05 | 0.337 |
| $\sigma(C^{31} - H^{55})$ | $\sigma^*(C^{46} - H^{50})$ | 57.08 | 4.6 | 0.458 |
| $\pi(C^{41}-C^{42})$ | $\pi^*(C^{24} = N^{33})$ | 12.85 | 0.28 | 0.056 |
| $\pi(C^{41}-C^{42})$ | π*(C ⁴³ – C ⁴⁶) | 19.55 | 0.29 | 0.068 |
| π(C ⁴¹ – C ⁴²) | π*(C ⁴⁴ – C ⁴⁸) | 19.21 | 0.28 | 0.067 |
| σ(C ⁴¹ – C ⁴³) | σ*(C ⁴¹ – C ⁴²) | 3.87 | 1.26 | 0.062 |
| σ(C ⁴² – C ⁴⁴) | $\sigma^*(C^{24}-C^{41})$ | 3.71 | 1.15 | 0.058 |
| σ(C ⁴² – C ⁴⁴) | σ*(C ⁴¹ – C ⁴²) | 3.39 | 1.27 | 0.059 |
| σ(C ⁴² – H ⁴⁵) | σ*(C ⁴¹ – C ⁴³) | 4.53 | 1.08 | 0.063 |
| $\sigma(C^{42}-H^{45})$ | σ*(C ⁴⁴ – C ⁴⁸) | 3.66 | 1.1 | 0.057 |
| σ(C ⁴³ – C ⁴⁶) | σ*(C ²⁴ – C ⁴¹) | 3.47 | 1.15 | 0.057 |
| $\sigma(C^{43}-C^{46})$ | σ*(C ⁴¹ – C ⁴³) | 3.31 | 1.27 | 0.058 |
| π(C ⁴³ – C ⁴⁶) | π*(C ⁴¹ – C ⁴²) | 19.66 | 0.28 | 0.067 |
| π(C ⁴³ – C ⁴⁶) | π*(C ⁴⁴ – C ⁴⁸) | 20.84 | 0.28 | 0.069 |
| $\sigma(C^{43}-H^{47})$ | σ*(C ⁴¹ – C ⁴²) | 4.73 | 1.08 | 0.064 |
| $\pi(C^{44}-C^{48})$ | π*(C ⁴¹ – C ⁴²) | 21.36 | 0.28 | 0.07 |
| π(C ⁴⁴ – C ⁴⁸) | π*(C ⁴³ – C ⁴⁶) | 18.87 | 0.29 | 0.066 |
| σ(C ⁴⁴ – H ⁴⁹) | π*(C ⁴¹ – C ⁴²) | 3.96 | 1.08 | 0.058 |
| σ(C ⁴⁶ – H ⁵⁰) | σ*(C ⁴¹ – C ⁴³) | 3.95 | 1.08 | 0.058 |
| σ(C ⁴⁶ – H ⁵⁰) | σ*(C ⁴⁴ – C ⁴⁸) | 3.65 | 1.09 | 0.057 |
| σ(C ⁴⁸ – H ⁵¹) | σ*(C ⁴² – C ⁴⁴) | 3.85 | 1.1 | 0.058 |
| σ(C ⁴⁸ – H ⁵¹) | σ*(C ⁴³ – C ⁴⁶) | 3.77 | 1.1 | 0.058 |
| n ₁ (N ³³) | $\sigma^*(C^{23}-H^{27})$ | 3.61 | 0.77 | 0.048 |
| n ₁ (N ³³) | $\sigma^*(C^{24}-C^{32})$ | 12.55 | 0.82 | 0.092 |
| n ₁ (N ³⁴) | $\pi^*(C^{25} = O^{39})$ | 56.51 | 0.27 | 0.113 |
| n ₁ (N ³⁴) | $\pi^*(C^{26}-C^{28})$ | 20.43 | 0.28 | 0.068 |
| n ₁ (N ³⁴) | $\sigma^*(C^{35} - H^{37})$ | 6.27 | 0.66 | 0.063 |

| Donor (i) | Acceptor (j) | E (2) | E(j) - E(i) | F _{i,j} |
|------------------------------------|--|----------|-------------|------------------|
| | | (kJ/mol) | (a.u) | (a.u) |
| n ₂ (O ³⁹) | σ*(C ²³ – C ²⁵) | 18.8 | 0.64 | 0.099 |
| n ₂ (O ³⁹) | $\sigma^*(C^{25} - N^{34})$ | 26.18 | 0.69 | 0.122 |
| n ₃ (Cl ⁴⁰) | $\pi^*(C^{29}-C^{30})$ | 11.23 | 0.34 | 0.06 |
| $\pi(C^{24} = N^{33})$ | $\pi^*(C^{31}-C^{32})$ | 51 | 0.02 | 0.056 |
| $\pi(C^{26}-C^{28})$ | $\pi^*(C^{31}-C^{32})$ | 93.19 | 0.03 | 0.082 |
| $\pi(C^{29}-C^{30})$ | $\pi^*(C^{31}-C^{32})$ | 83.36 | 0.04 | 0.085 |
| $\pi(C^{41}-C^{42})$ | $\pi^*(C^{31}-C^{32})$ | 4.14 | 0.02 | 0.012 |

Table S-2 (part 3): Second-order perturbation theory analysis of Fock Matrix in NBO Basis of Dopamine - Diazepam biomolecular complex to understand the intra and intermolecular charge transfer.



| Mode | Raman Expt. | FTIR Expt. | Scaled Wave- number | Vibrational Assignments |
|------|----------------|---------------|---------------------------|--|
| 1 | 3592 | 3597 | 3589 | υ(O ¹⁰ – H ¹¹)99, υ(O ¹² – H ¹³)76 |
| 2 | 3350 | 3338 | 3310 | $υ(N^{19}-H^{20})100$, $υ(N^{19}-H^{21})100$ |
| 3 | 2869 | 2869 | 2879 | υ(C ¹ – H ⁷)82 |
| 4 | 2634 | 2541 | 2559 | $\beta(H^7 - C^1 - C^2)78$ |
| 5 | | 1621 | 1672 | $\upsilon(O^{10}-H^{11})20$, $\tau(H^{11}-O^{10}-C^6-C^5)13$ |
| 6 | 1612 | | 1615 | $\tau(H^{11}-O^{10}-C^6-C^5)11$, $\upsilon(C^4-H^9)16$ |
| 7 | 1541 | | 1540 | $υ(C^{14} - H^{15})12$, $β(H^9 - C^4 - C^3)16$ |
| 8 | 1448 | 1497 | 1421 | $\beta(H^9-C^4-C^3)12$, $\tau(H^{17}-C^{16}-C^{14}-C^3)23$ |
| 9 | | 1345 | 1334 | υ(C ¹⁴ – H ¹⁵)15 |
| 10 | | | 1322 | $\beta(H^{13}-O^{12}-C^5)15$, $\tau(H^{12}-O^{13}-C^5-C^4)18$, $\tau(H^9-C^4-C^3-C^{14})11$ |
| 11 | 1286 | 1284 | 1260 | $\tau(H^{15}-C^{14}-C^3-C^4)10$, $\upsilon(O^{10}-H^{11})12$ |
| 12 | 1200 | 1206 | 1213 | $\beta(H^9 - C^4 - C^3)16$, $\tau(H^{11} - O^{10} - C^6 - C^5)11$, $\tau(H^9 - C^4 - C^3 - C^{14})22$ |
| 13 | 1150 | 1147 | 1138 | $\beta(H^{17}-C^{16}-N^{19})11$ |
| 14 | 1115 | 1076 | 1083 | $\beta(H^{17}-C^{16}-N^{19})16$, $\upsilon(C^{16}-H^{17})11$, $\upsilon(C^{16}-H^{18})15$ |
| 15 | 961 | 937 | 916 | $\beta(C^6-C^5-C^4)11$, $\beta(C^2-C^1-C^6)12$, $\upsilon(C^4-C^5)10$, $\upsilon(C^2-C^3)16$ |
| 16 | | 876 | 874 | $\upsilon(C^5-C^6)15$, $\tau(C^1-C^6-C^5-C^4)22$, $\gamma(O^{12}-C^4-C^6-C^5)11$ |
| 17 | | 815 | 811 | $ \frac{\tau(C^2-C^1-C^6-C^5)11,\ \tau(C^1-C^6-C^5-C^4)12,\ \beta(C^1-C^6-C^5)10,}{\gamma(O^{10}-C^5-C^1-C^6)33} $ |
| 18 | 790 | 788 | 783 | $v(C^1-C^2)15$, $\beta(C^1-C^2-C^3)11$ |
| 19 | | | 757 | $\upsilon(C^1 - C^6)17$, $\upsilon(C^2 - C^3)15$ |
| 20 | | | 717 | $\beta(O^{12}-C^5-C^6)16$ |
| 21 | 746 | 704 | 707 | $\beta(H^{20}-N^{19}-C^{16})15$, $\omega(N^{19}-H^{20}-H^{21})19$, $\omega(N^{19}-H^{20}-H^{21})13$ |
| 22 | | | 686 | $\beta(C^{14}-C^3-C^2)16$ |
| 23 | | | 662 | $\beta(C^{14}-C^3-C^2)13$, $\tau(H^{18}-C^{16}-C^{14}-C^3)11$ |
| 24 | 634 | 629 | 630 | $\upsilon(N^{19}-H^{20})15,\beta(H^{20}-N^{19}-C^{16})17,\tau(H^{22}-C^{14}-C^3-C^4)12$ |
| 25 | 594 | 597 | 595 | $\upsilon(C^{14}-C^{16})10$, $\beta(H^{15}-C^{14}-C^{16})15$, $\beta(H^{22}-C^{14}-H^{15})10$ |
| 26 | | | 582 | $\tau(N^{19}-C^{16}-C^{14}-C^3)23$, $\tau(C^{16}-C^{14}-C^3-C^4)17$ |
| 27 | | | 571 | $\beta(C^{16}-C^{14}-C^3)11$, $\beta(H^{18}-C^{16}-H^{17})12$, $\upsilon(N^{19}-C^{16})18$ |
| 28 | | 531 | 537 | $\beta(H^{17}-C^{16}-N^{19})$ 10, $\beta(H^{18}-C^{16}-H^{17})$ 12, $\tau(H^{20}-N^{19}-C^{16}-C^{14})$ 13 |
| 29 | | | 515 | $τ(H^{21} - N^{19} - C^{16} - C^{14})18$, $υ(N^{19} - C^{16})11$, $υ(C^{14} - H^{22})20$ |
| 30 | 477 | | 473 | υ(C ¹⁴ – H ²²)21 |
| 31 | | 426 | 431 | $\beta(H^{21}-N^{19}-H^{20})21$, $\tau(H^{18}-C^{16}-C^{14}-C^3)15$, $\upsilon(N^{19}-H^{21})12$ |
| 32 | 394 | | 351 | $\tau(H^{22}-C^{14}-C^3-C^4)23$, $\upsilon(N^{19}-H^{21})10$ |
| 33 | 267 | | 229 | $\beta(N^{19}-C^{16}-C^{14})$ 13, $\beta(C^{16}-C^{14}-C^{3})$ 12 |
| 34 | 200 | | 202 | $\tau(N^{19}-C^{16}-C^{14}-C^3)22$, $\tau(C^{16}-C^{14}-C^3-C^4)32$ |

Table S-3a: Theoretical and experimental wavenumbers (cm^{-1}) and potential energy distribution for vibrational modes of Dopamine to understand the type of vibrations for identifying the compositions.



| Мо- | Raman | FTIR | Scaled | Vibrational Assignments |
|-----|-------|-------|--------|--|
| de | Expt. | Expt. | Wave- | |
| | • | • | number | |
| 1 | 3052 | 3000 | 3104 | $υ(C^1 - H^5)27$, $β(H^5 - C^1 - N^{11})61$ |
| 2 | 2937 | 2894 | 2916 | $v(C^1 - H^5)57$, $\beta(H^5 - C^1 - N^{11})26$ |
| 3 | 2832 | 2807 | 2808 | $v(C^1 - H^5)13$, $\tau(H^5 - C^1 - N^{11} = C^2)71$ |
| 4 | 2676 | 2709 | 2673 | $\upsilon(C^{13}-H^{16})29$, $\upsilon(C^{13}-H^{15})20$, $\beta(H^{16}-C^{13}-H^{15})15$, $\tau(H^{23}-C^{20}-H^{15})15$ |
| | | | | $C^{22} - C^{26}$)11 |
| 5 | | | 2222 | $υ(C^6 - H^{30})29$, $ν(C^{24} - H^{28})21$, $β(H^{30} - C^6 - C^7)14$, $τ(H^{31} - C^1 - N^{11} = C^2)13$ |
| 6 | | 1827 | 1893 | $ \begin{array}{l} \upsilon(C^{24}-H^{28})13,\beta(H^{27}-C^{22}-C^{26})14,\tau(H^{27}-C^{22}-C^{26}-C^{24})13,\tau(H^{28}-C^{24}-C^{26}-C^{22})13 \end{array} $ |
| 7 | 1772 | 1771 | 1742 | $v(C^1 - H^{31})25$ |
| 8 | | | 1735 | $υ(C^1 - H^{31})20$, $β(H^{30} - C^6 - C^7)10$, $τ(H^{30} - C^6 - C^7 - C^8)11$, $τ(H^{29} - C^{26} - C^{24} - C^{21})10$ |
| 9 | 1680 | 1684 | 1664 | $\upsilon(C^3 = O^{17})77$, $\upsilon(C^1 - H^{31})12$, $\tau(H^{28} - C^{24} - C^{26} - C^{22})41$ |
| 10 | 1658 | | 1658 | $\tau(H^{27}-C^{22}-C^{26}-C^{24})49$ |
| 11 | | 1550 | 1537 | $\upsilon(C^{24}-H^{28})12, \beta(H^{30}-C^6-C^7)16$ |
| 18 | 1345 | 1389 | 1360 | $\tau(H^{29}-C^{26}-C^{24}-C^{21})12$ |
| 13 | 1267 | | 1298 | $\beta(H^{33}-C^9-C^{10})12$, $\beta(H^{25}-C^{21}-C^{24})11$, $\tau(H^{25}-C^{21}-C^{24}-C^{26})12$ |
| 14 | | | 1262 | $\upsilon(C^{20}-H^{23})17$, $\beta(H^{25}-C^{21}-C^{24})27$, $\tau(H^{25}-C^{21}-C^{24}-C^{26})21$ |
| 15 | 1238 | 1206 | 1233 | $\beta(H^{32}-C^7-C^8)14$, $\tau(H^{14}-C^{13}-N^{12}-C^4)15$ |
| 16 | 1132 | 1142 | 1167 | $\beta(H^{32}-C^7-C^8)10$, $\tau(H^{25}-C^{21}-C^{24}-C^{26})27$ |
| 17 | 1088 | 1096 | 1063 | $\beta(H^{32}-C^7-C^8)25$ |
| 18 | 1042 | 1034 | 1022 | $\tau(C^8 = C^9 - C^{10} - C^2)11, \tau(C^7 - C^8 = C^9 - C^{10})11$ |
| 19 | 1020 | | 1000 | $\tau(H^{32} - C^7 - C^8 = C^9)12$ |
| 20 | | 988 | 984 | $v(C^4 - C^6)17$ |
| 21 | | 944 | 962 | $\tau(C^8 = C^9 - C^{10} - C^2)12, \tau(C^7 - C^8 = C^9 - C^{10})12$ |
| 22 | 925 | 902 | 917 | $v(C^9 - C^{10})19$ |
| 23 | 854 | | 851 | $υ(C^7 - C^8)14$, $β(C^6 - C^7 - C^8)11$, $β(C^7 - C^8 = C^9)11$, $β(C^8 = C^9 - C^{10})11$ |
| 24 | 786 | | 782 | $v(C^8 - Cl^{18})15$ |
| 25 | 758 | 739 | 738 | $\tau(C^6-C^7-C^8=C^9)10, \tau(C^4-C^6-C^7-C^8)12, \tau(C^9-C^{10}-C^2-C^9)12, \tau(C^{13}-N^{12}-C^4-C^6)10$ |
| 26 | | | 728 | $\tau(C^6 - C^7 - C^8 = C^9)12$, $\tau(C^4 - C^6 - C^7 - C^8)14$, $\tau(C^9 - C^{10} - C^2 - C^{19})14$ |
| 27 | | 707 | 711 | $\tau(C^1 - N^{11} = C^2 - C^{10})23$ |
| 28 | 700 | | 701 | $v(C^1 - N^{11})22$ |
| 29 | | | 690 | $v(C^1 - N^{11})17$, $\beta(H^{33} - C^9 - C^{10})12$ |
| 30 | 631 | 634 | 644 | $\beta(C^{19}-C^{20}-C^{22})27$ |
| 31 | | 560 | 550 | $v(C^{19}-C^{20})23$ |
| 32 | | 516 | 539 | $v(C^9 - C^{33})11$ |
| 33 | 483 | 488 | 495 | $\beta(C^{21}-C^{24}-C^{26})25$, $\beta(C^2-C^{19}-C^{21})10$, $\beta(C^{10}-C^2-C^{19})11$ |
| 34 | | 448 | 448 | $\tau(H^{25}-C^{21}-C^{24}-C^{26})12,\;\tau(C^{21}-C^{24}-C^{26}-C^{22})29,\tau(C^{24}-C^{26}-C^{22}-C^{20})11$ |
| 35 | 362 | | 379 | $υ(N^{12}-C^{13})33$, $β(C^3-N^{12}-C^4)16$, $β(N^{12}-C^4-C^6)16$, $β(C^{13}-N^{12}-C^3)14$ |
| 36 | 258 | | 266 | $v(C^7 - H^{32})17$ |

Table S-3b: Theoretical and experimental wavenumbers (cm^{-1}) and potential energy distribution for vibrational modes of Dopamine to understand the type of vibrations for identifying the compositions.



References

- [1] J. France, Springer, Boston, MA, 92 (1991).
- [2] C. Kuehner, Acta. Psychiatr. Scand. 108, 163 (2003).
- [3] R. M. Rapee, C. A. Schniering, J. L. Hudson, Annu. Rev. Clin. Psychol. 5, 311 (2009).
- [4] M. Zeidner, International Encyclopedia of Education, 3rd Edition, 549 (2010).
- [5] S. Rachman, Anxiety, 2nd ed., Oxford: Blackwell (2004).
- [6] M. Zarrindast, F. Khakpai, Arch. Iran. Med. 18, 591 (2015).
- [7] M. O. Klein, D. S. Battagello, A. R. Cardoso, D. N. Hauser, J.C. Bittencourt, R. G. Correa, Cell. Mol. Neurobiol. 39, 31 (2019).
- [8] I. Fidianingsih, T. Nurmasitoh, A.Z. Arjana, N. Devita, U. Khoiriyah, Univ. Med. 38, 48 (2019).
- [9] B. Bandelow, S. Michaelis, Clin. Neurosci. Res. 17, 327 (2015).
- [10] V. V. Zakusov, S. N. Ostrovskaya, V. V. Markovich, G. M. Molodavkin, T. A. Voronina, Arch. Int. Pharmacodyn. Ther. 229, 313 (1977).
- [11] J. W. Tiller, I. Schweitzer, K. P. Maguire, B. Davis, B. J. Psych. 155, 483 (1989).
- [12] D. J. Nutt, A. L. Malizia, B. J. Psych. 179, 390 (2001).
- [13] A. Alexander Gomez, M. Amanda Fiorenza, L. Suelen Boschen, H. Adam Sugi, D. Beckman, T. Sergio Ferreira, K. Lee, D. Charles Blaha, C. Da Cunha, ACS Chem. Neurosci. 8, 300 (2017).
- [14] D. J. Greenblatt, R. I. Shader, Drug Metab. Rev. 8, 13 (1978).
- [15] A. Catherine Christian, G. Anne Herbert, L. Rebecca Holt, P. Kathy, D. Kyla Sherwood, S. Pangratz-Fuehrer, R. Uwe, R. John Huguenard, Neuron 78, 1063 (2013).
- [16] C. Zhai, H. Ma, F. Sun, L. Li, A. Song, 215, 481 (2016).
- [17] C. P. Zhai, P. Peng, X. J. Liu, X. Chen, L. N. Li, J. Mol. Struct. 1178, 599 (2019).
- [18] C. P. Zhai, F. Sun, P. Zhang, H. T. Ma, A. X. Song, J. C. Hao, J. Mol. Liq. 223, 420 (2016).
- [19] P. Zhang, P. Peng, B. B. Hou, C. P. Zhai, J. Phys. Chem. Lett. 57, 746 (2019).
- [20] Y. Y. Li, C. C. Chiu, J.J. Wang, Y. W. Chen, C. H. Hung, Pharmacol. Rep. 71, 732 (2019).
- [21] J. Li, H. Y. Duan, W. Z. Wei, S. L. Luo, Phys. Chem. Liq. 50, 453 (2012).
- [22] R. Djemil, D. Khatmi, J. Comput. Theor. Nanosci. 9, 1571 (2012).
- [23] M. M. Liu, S. M. Han, X. W. Zheng, L. L. Han, T. Liu, Z. Y. Yu, Int. J. Electrochem. Sci. 10, 235 (2015).
- [24] D. John Roache, R. Roland Griffiths, Pharmacol. Biochem. Behav. 26, 801 (1987).
- [25] A.L. van Steveninck, R. Gieschke, H.C. Schoemaker, M.S.M. Pieters, J.M. Kroon, D.D. Breimer, A.F. Cohen, Psychopharmacol. 110, 471 (1993).
- [26] U. Laisi, M. Linnoila, T. Seppfil i, J.-J. Himberg, M.J. Mattila, Eur. J. Clin. Pharmacot. 16, 263 (1979).
- [27] Z. Esmaeeli, M. Reza Khodabakhshi, Z. Mirjafary, H. Saeidian, J. Mol. Struct. 1246, 131206 (2021).
- [28] F. Qashu, T.H. Figueiredo, V. Aroniadou-Anderjaska, J.P. Apland, M.F. Braga, Amino Acids. 38, 189 (2010).
- [29] A. Igarashi, N. Zadzilka, M. Shirahata, Adv. Exp. Med. Biol. 648, 169 (2009).



- [30] J. Riss, J. Cloyd, J. Gates, S. Collins, Acta Neurol. Scand. 118, 69 (2008).
- [31] A. Acikgoz, N. Karim, S. Giri, W. Schmidt-Heck, A. Bader, Appl. Pharm. 234, 179 (2009).
- [32] T. Inaba, A. Tait, M. Nakano, W.A. Mahon, W. Kalow, Drug Metab. Dispos. 16, 605 (1998).
- [33] G. Bruni, M. Maietta, V. Berbenni, P. Mustarelli, C. Ferrara, M. Freccero, V. Grande, L. Maggi, C. Milanese, A. Girella, A. Marini, J. Phys. Chem. B. 118, 9180 (2014).
- [34] Ch. Sonia, N. Chetry, Th. Gomti Devi, T. Karlo, J. Mol. Struct. 1295, 136656 (2024).
- [35] G. Bruni, M. Maietta, V. Berbenni, P. Mustarelli, C. Ferrara, M. Freccero, V. Grande, L. Maggi, C. Milanese, A. Girella, A. Marini, J. Phys. Chem. B. 118, 9180 (2014).
- [36] Z. Huang, H. Lui, X. K. Chen, A. Alajlan, D. I. McLean, H. Zeng, J. Biomed. Opt. 9, 1198 (2004).
- [37] K. R. Strehle, D. Cialla, P. Rösch, T. Henkel, M.K. Köhler, J. A. Popp, Anal. Chem. 79, 1542 (2007).
- [38] H. Putz, K. Brandenburg GbR Kreuzherrenstr. Crystal Impact 102, 53227.
- [39] M. J. Frisch, G. W. Trucks, H. B. Schlegel, G. E. Scuseria, et al., Gaussian 16, Revision C 0.02. Gaussian, Inc., Wallingford CT 2019.
- [40] F. Ban, K. N. Rankin, J. W. Gauld, R.J. Boyd, Theor. Chem. Acc. 108, 1 (2002).
- [41] J. P. Merrick, D. Moran, L. Radom, J. Phys. Chem. A. 111, 11683 (2007).
- [42] N. Uludag, G. Serdaroglu, A. Yinanc, J. Mol. Struct. 1161, 152 (2018).
- [43] A. Joshua, Plumley, J.J. Dannenberg, J. Comput. Chem. 32, 1519 (2011).
- [44] R. Cammi, Molecular Response Functions for the Polarizable Continuum Model, Springer, 2013.
- [45] Y. Takano, K. N. Houk, J. Chem. Theory Comput. 1, 70 (2005).
- [46] A. V. Marenich, C. J. Cramer, D.G. Truhlar, J. Phys. Chem. B. 113, 6378 (2009).
- [47] V. Barone, M. J. Cossi, Phys. Chem. A. 102, 1995 (1998).
- [48] E. Cances, B. Mennucci, J. Tomasi, J. Chem. Phys. 107, 3032 (1997).
- [49] A. Sagaama, N. Issaoui, O. Al-Dossary, S. Aleksandr Kazachenko, J. Marek Wojcik, J. King Saud Univ. Sci. 33, 101606 (2021).
- [50] M. H. Jamroz, Spectrochimica Acta A. 114, 220 (2013).
- [51] M. T. Rosado, M. Leonor, T. S. Duarte, R. Fausto, Vib. Spectrosc. 16, 35 (1998).
- [52] A. D. Mackerell, D. Bashford, M. Bellot, R. L. Dunbrack, J. D. Evanseck, M. J. Field, S. Fischer, J. Gao, H. Guo, S. Ha, D. J. McCarthy, L. Kuchnir, K. Kuczera, F. T. K. Lau, C. Mattos, S. Michnik, T. Ngo, D.T. Nguyen, B. Prodhom, W.E. Reiher, B. Roux, M. Schlenkrich, J. C. Smith, J. Straub, R. Stole, J. D. Yin Watanable, M. Karplus, J. Phys. Chem. B. 102, 3586 (1998).
- [53] N. M. O'Boyle, A.L. Tenderholt, K. M. Langner, J. Comput. Chem. 29, 839 (2008).
- [54] Th. Gomti Devi, K. Kumar, J. Raman Spectrosc. 35, 835 (2004).
- [55] G. Upadhayay, Th. Gomti Devi, J. Mol. Liq. 197, 263 (2014).
- [56] M. Al. Khaldun Azzam, Complex use of Mineral Resources. 325, 14 (2023).
- [57] G. M. Morris, R. Huey, W. Lindstrom, F. M. Sanner, K. R. Belew, S.D. Goodsell, A.J. Olson, J. Comput. Chem. 30, 2785 (2009).
- [58] P. Folorunsho Ayodele, A. Toyin Bamigbade, O. Omolara Bamigbade, A. Isaac Abiodun, T. Esther Shiminenge, S. Abiodun Joseph, F. Samuel Tobi, Prog. Drug Discov. Biomed. Sci. 6, 1 (2023).



- [59] T. Lu, F. Chen, J. Comput. Chem. 33, 580 (2012).
- [60] W. Humphrey, A. Dalke, K. Schulten, J. Mol. Graph. 14, 27 (1996).
- [61] B. Priyanka, O. Andreas Eckert, K. Anna Schrey, R. Preissner, Nucleic Acids Res. 46, 257 (2018).
- [62] J. Saikia, Th. Gomti, T. Karlo, J. Mol. Struct. 1250, 131889 (2022).
- [63] N. Chetry, Th. Gomti, T. Karlo, J. Mol. Struct. 1250, 131670 (2022).
- [64] N. Chetry, Th. Gomti, J. Mol. Liq. 338, 116689 (2021).
- [65] B. Borah, Th. Gomti, J. Mol. Struct. 1210, 128022 (2020).
- [66] B. Borah, Th. Gomti, J. Mol. Struct. 1221, 128819 (2020).
- [67] B. Borah, Th. Gomti, J. Mol. Struct. 1203, 127396 (2020).
- [68] J. Saikia, B. Borah, Th. Gomti, J. Mol. Struct. 1227, 129664 (2021).
- [69] H. Gökce, N. Öztuk, Y.B. Alpaslan, M. Tasan, G. Alpaslan, Spectrosc. Lett. 49, 167 (2016).
- [70] R. G. Pearson, Chemistry (Easton). 27, 734 (1998).
- [71] J. M. Mikhail Glukhovtsev, S. Seminario, J. Chem. Inf. Comput. 37, 6 (1997).
- [72] P. Politzer, P.R. Laurence, K. Jayasuria, Environ. Health Perspect. 61, 191 (1985).
- [73] M. Boopathi, P. Udhayakala, T.V. Rajendiran, S. Gunasekaran, Appl. Spectrosc. 83, 12 (2016).
- [74] P. Suraj Singh, Th. Gomti, J. Mol. Struct. 1305, 137709 (2024).
- [75] L. Willingson, P. Suraj Singh, Th. Gomti, J. Mol. Struct. 1308, 137962 (2024).
- [76] T. N. Rekha, R. M. Asath, B. J. M. Rajkumar, S. Premkumar, A. Jawahar, T. Mathavan, A. M. F. Benial, Spectrosc. Lett. 49, 155 (2016).
- [77] K. Fukui, Amer. Assoc. Adv. Sci. 218, 747 (1982).
- [78] T. Koopman, Physica. 1, 104 (1934).
- [79] A. Jeelani, B. Narayana, S. Muthu, J. Mol. Struct. 1241, 130558 (2021).
- [80] N. Chetry, T. Karlo, Th. Gomti, J. Mol. Struct. 1266, 133410 (2022).
- [81] J. Saikia, Th. Gomti Devi, T. Karlo, J. Mol. Struct. 1286, 135546 (2023).
- [82] Th. Gomti Devi, Th. Joymati Devi, P. Suraj Singh, L. Willingson, J. Mol. Liq. 397, 124055 (2024).
- [83] A. N. Tahneh, S. B. Novir, E. Balali, J. Mol. Model. 23, 356 (2017).
- [84] J. Saikia, T. Gomti Devi, T. Karlo, J. Mol. Struct. 1283, 135208 (2023).
- [85] G. Wagniere, Appl. Phys. B. 41, 169 (1986).
- [86] R. N. Singh, P. Rawat, A. Kumar, P. Kant, A. Srivastava, Spectrosc. Lett. 48, 235 (2017).
- [87] D. A. Kleinmann, Phys. Rev. 12, 61977 (1962).
- [88] R. Mathanmal, N. Sudha, L. G. Prasad, N. Ganga, V. Krishnakumar, Spectrochim. Acta A. 137, 740 (2015).
- [89] V. C. Kishore, R. Dhanya, R. Sreekumar, R. Joseph, C.S. Kartha, Spectrochim. Acta A. 70, 1227 (2008).
- [90] P. Subhapriya, K. Sadasivam, P. Pachamuthu, V. Dhanapal, P. S. Vijayanand, Mol. Cryst. Liq. Cryst. 650, 65 (2017).
- [91] J. Saikia, N. Chhetry, Th. Gomti, Spectrosc. Lett. 57(5), 300 (2024).



- [92] S. S. Mishra, Int. J. Pharm. Phytopharmacol Res. 6, 77 (2016).
- [93] C. A. Lipinski, F. Lombardo, B. W. Dominy, P.J. Feeney, Adv. Drug Deliv. Rev. 46, 3 (2001).
- [94] M. Bayat, F. Yaghoobi, S. Salehzadeh, S. Hokmi, Polyhedron. 30, 2809 (2011).
- [95] K. Sangeetha, S. R. Rajina, M. K. Marchewka, J. Binoy, Mater. Today Proc. 25, 307 (2020).
- [96] A. Srivastava, R. Mishra, B.D. Joshi, V. Gupta, P. Tandon, Mol. Sim. 40, 1099 (2014).
- [97] O. Noureddine, N. Issaoui, M. Medimagh, O. Al-Dossary, H. Marouani, J. King Saud Univ. Sci. 33, 101334 (2021).
- [98] M. R. Sameti, P. Zarei, Adsorption. 24, 757 (2018).
- [99] U. Koch, P. L. A. Popelier, J. Phys. Chem. 99, 9747 (1995).
- [100] E. Espinosa, E. Molins, C. Lecomte, Chem. Phys. Lett. 285, 170 (1998).
- [101] K. Anitha, V. Balachandran, B. Narayan, Int. J. Curr. Res. Acad. Rev. 3, 70 (2015).
- [102] G. Saleh, C. Gatti, L.L. Presti, J. Contreras-García, Chem. Eur. J. 18, 15523 (2012).
- [103] T. Mackoy, B. Kale, E. Michael Papka, R. Wheeler, Comput. Phys. Commun. 264, 107881 (2021).
- [104] P. Wu, R. Chaudret, X. Hu, W. Yang, J. Chem. Theor. Comput. 9, 2226 (2013).
- [105] J. Contreras-García, R.A. Boto, F. Izquierdo-Ruiz, I. Reva, T. Woller, M. Alonso, Theor. Chem. Acc. 135, 242 (2016).
- [106] M. N. Drwal, P. Banerjee, M. Dunkel, M.R. Wettig, R. Preissner, Nucleic Acids Res. 42, 53 (2014).
- [107] S. Tian, J. Wang, Y. Li, D. Li, L. Xu, T. Hou, Adv. Drug Deliv. Rev. 86, 2 (2015).
- [108] M. Mukunda, B. Borah, Th. Gomti Devi, J. Mol. Struct. 1163, 205 (2018).
- [109] Z. Kevizano Jacinta, V. Mathivanan, G. Hezinglila, D. Leelavathi, Int. J. Pharm. Investig. 12, 418 (2022).
- [110] G. Upadhyay, P. Upadhyay, Th. Gomti Devi, J. Raman Spectrosc. 46, 1291 (2015).
- [111] S. Sevvanthi, S. Muthu, M. Raja, J. Mol. Struct. 1149, 487 (2017).
- [112] Ch. Sonia, Th. Gomti Devi, T. Karlo, J. Mol. Struct. 1223, 128972 (2020).
- [113] B. Borah, Th. Gomti Devi, J. Mol. Struct. 1223, 128972 (2020).
- [114] P. Suraj Singh, Th. Gomti Devi, Spectrosc. Lett.
- [115] A. B. Dempster, J. Mol. Spectrosc. 36, 18 (1970).
- [116] P. Manimaran, S. Balusubramaniyan, M. Azam, D. Rajadurai, S.I. Al-Resayes, G. Mathubala, A. Manikandan, S. Muthupandi, Z. Tabassum, I. Khan, Molecules. 26, 823 (2021).
- [117] H. Xue-Qin, Z. Hua, W. Fang, G. Tian, X. Zhe-Kun, W. Zhong-Xia, J. Phys. Chem. Lett. 12, 5221 (2021).
- [118] A. Andrey Buglak, I. Alexeim Kononov, RSC Adv. 10, 34149 (2010).
- [119] J. Fan, A. Fu, L. Zhang, Quant. Biol. 7, 83 (2019).
- [120] J. Adhikari Subin, R. Lal Swagat Shrestha, Cell Biochem. Biophys. 82, 3413 (2024).
- [121] P. Yadav, M. Rana, P. Chowdhury, J. Mol. Struct. 1246, 131253 (2021).